

Gamma Ray Heating and Neutrino Cooling Rates due to Weak Interaction Processes on *sd*-shell Nuclei in Stellar Cores

Muhammad Fayaz¹ • Jameel-Un Nabi¹ •
Muhammad Majid¹

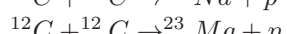
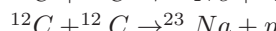
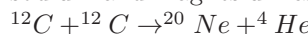
Abstract Gamma ray heating and neutrino cooling rates, due to weak interaction processes, on *sd*-shell nuclei in stellar core are calculated using the proton neutron quasiparticle random phase approximation theory. The recent extensive experimental mass compilation of (Wang et al. 2012), other improved model input parameters including nuclear quadrupole deformation (Raman et al. 2001), (Möller et al. 2016) and physical constants are taken into account in the current calculation. The purpose of this work is two fold, one is to improve the earlier calculation of weak rates performed by (Nabi & Klapdor-Kleingrothaus 1999) using the same theory. We further compare our results with previous calculations. The selected *sd*-shell nuclei, considered in this work, are of special interest for the evolution of O-Ne-Mg core in 8–10 M_⊙ stars due to competitive gamma ray heating rates and cooling by URCA processes. The outcome of these competitions is to determine, whether the stars end up as a white dwarf (J. -U. Nabi 2008), an electron-capture supernova (Jones et al. 2013) or Fe core-collapse supernova (Suzuki et al. 2016). The selected *sd*-shell nuclei for calculation of associated weak-interaction rates include ^{20,23}O, ^{20,23}F, ^{20,23,24}Ne, ^{20,23–25}Na, and ^{23–25}Mg. The cooling and heating rates are calculated for density range ($10 \leq \rho(\text{g.cm}^{-3}) \leq 10^{11}$) and temperature range ($0.01 \times 10^9 \leq T(K) \leq 30 \times 10^9$). The calculated gamma heating rates are orders of magnitude bigger than the shell model rates (except for ²⁵Mg at low densities). At high temperatures the gamma heating rates are in rea-

sonable agreement. The calculated cooling rates are up to an order of magnitude bigger for odd-A nuclei.

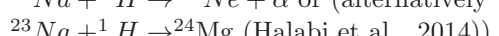
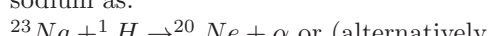
Keywords gamma ray heating rates; neutrino cooling rates; *sd*-shell nuclei; pn-QRPA theory; stellar evolution; core-collapse.

1 Introduction

In stars, as massive as (8–10) M_⊙, the helium burning phase brings some crucial changes for further evolution of the core (Woosley et al. 2002): 1- The carbon and oxygen (C-O) core grows via triple alpha reaction and alpha capture on carbon synthesizes oxygen. 2- Subsequent α -capture causes the formation of ²⁰Ne and a little ²⁴Mg. After the helium burning phase, the temperature and density increase progressively and can evolve into advance burning stages. The core of carbon and oxygen contracts, the temperature reaches $\sim 5 \times 10^8 \text{K}$ and density $\sim 3 \times 10^6 \text{ g.cm}^{-3}$ (Ryan 2010). The carbon-carbon fusion begins to create neon, sodium and magnesium as follows:



The free protons thus produced, may add onto the sodium as:



These reactions show that the core of massive star, after carbon burning phase, comprises mainly of oxygen-16 (¹⁶O), ²⁰Ne and ²⁴Mg. ¹⁶O, due to its high Coulomb barrier, survives the carbon burning phase and later captures α -particles to transform into ²⁰Ne. Other derivative reactions of carbon burning phase are the neutron-capture, proton-capture and alpha captures to synthesize isotopes like ²¹Ne, ²²Ne, ²⁵Mg, ²⁶Al

Muhammad Fayaz

Jameel-Un Nabi

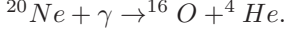
Muhammad Majid

¹Faculty of Engineering Sciences,
GIK Institute of Engineering Sciences and Technology, Topi
23640, Khyber Pakhtunkhwa, Pakistan.

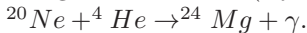
¹Corresponding author email : jameel@giki.edu.pk

(unstable), ^{29}Si , ^{30}Si and ^{31}P (Woosley et al. 2002). The relative abundance of these species can be seen in Ref. (García et al. 1997).

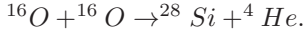
^{16}O being a double magic nucleus, is therefore very stable and its fusion can not trigger at temperatures below $2 \times 10^9 \text{ K}$. Before the oxygen fusion phase, at temperature $\sim 1.2 - 1.8 \times 10^9 \text{ K}$, neon burning takes place; by absorbing high energy gamma ray and disintegrates to ^{16}O and α particle spontaneously



The helium nuclei thus produced, react with other existing neon nuclei as (Ryan 2010):



At the end of neon burning phase, the stellar core mainly comprises of ^{16}O and ^{24}Mg nuclei. In high mass stars ($> 10 M_\odot$), the core temperature can exceed $2 \times 10^9 \text{ K}$, and oxygen burning (O-O fusion) can trigger via the reaction:



Stars in mass range $8-12 M_\odot$ may not proceed towards oxygen burning phase and are thought to form an O-Ne-Mg core interior to a helium core of $2-3 M_\odot$ after the carbon burning phase (Miyaji et al. 1980). In later works, e.g. (Woosley & Weaver 1980), (Nomoto 1987) and (Miyaji & Nomoto 1987), the favorable mass range for an O-Ne-Mg core shifted to $8-10 M_\odot$. They reported that stars in this mass range develop an electron-degenerate O-Ne-Mg core after the carbon burning. The electron captures begin on ^{24}Mg and ^{24}Na first, and later on ^{20}Ne and ^{20}F . This causes a loss of degeneracy pressure support (Martínez-Pinedo et al. 2014). Such stars can end up their lives in variety of ways, e.g., as O-Ne-Mg white dwarfs without explosion or accretion induced collapse, an electron-capture supernovae (ECSN) or Fe core-collapse supernovae (Fe-CCSN) (Suzuki et al. 2016). Supernovae Type Ia (SNe Ia) are, supposedly the explosive events of accreting white dwarfs. Due to relatively high Fermi energy of the degenerate electron gas, such white dwarfs trigger the electron capture process and reduce the lepton fraction significantly (J. -U. Nabi 2008).

In ECSN or Fe-CCSN scenario, the electron capture causes a rapid contraction of the electron-degenerate O-Ne-Mg core. The competing processes like contraction; cooling, and heating control the evolutionary changes in the central density and temperature, (Suzuki et al. 2016). If heating is fast enough relative to contraction, the temperature would become high enough to ignite Ne-O burning, which would proceed towards the Fe core formation. If cooling is fast, the contraction would lead to the collapse of the O-Ne-Mg core and an electron-capture supernova. The last episode of the life of 8-10

M_\odot stars is thus set by these competitions, which are induced by electron capture and β -decay. Therefore the accurate weak rates and, related neutrino cooling and gamma ray heating rates are of decisive importance for determination of the thermodynamic and hydrodynamic trajectory of stars in the late stages of their evolution. Such stars, ultimately, ignite Ne and O explosively at central density $\sim 2 \times 10^{10} \text{ g.cm}^{-3}$ and the core approaches to Chandrasekhar mass (Gutiérrez et al. 2005) and evolve into core collapse scenario due to electron capture on ^{20}Ne and ^{24}Mg (Nomoto 1987).

According to Ref. (Miyaji et al. 1980), much entropy is produced by γ ray emission from the excited states of daughter nuclei and by distortion in electron distribution function, as the after effect of electron capture. The emitted γ rays heat up the core material and cause the convection as well (Takahara et al. 1989). The temperature of the core is now high enough to ignite oxygen deflagration. The O-Ne-Mg core grows towards the Chandrasekhar mass, the electron capture on the post-deflagration material continues, which determines either explosion or collapse, as the final outcome of the star.

Weak interaction processes in massive stars constitute the energy budget in the last stages of stellar life. Ref. (Gupta et al. 2007) have shown that cooling by weak interaction neutrinos is remarkably reduced by the heating effect due to electron captures and the following γ -ray emission. Owing to core mass and its composition, these reactions can release up to a factor of 10 times more heat at densities $\sim 10^{11} \text{ g.cm}^{-3}$. Thus neutrinos take enormous energy from the transparent core of the star for stellar densities $\sim 10^{11} \text{ g.cm}^{-3}$ but gamma rays, on the other hand, are trapped in the stellar core and heat up the matter. This competition plays its part towards the oxygen deflagration and initiate convection in the core as well.

In this work gamma heating and (anti)neutrino cooling rates, due to weak rates on sd -shell nuclei, are calculated using proton-neutron Quasiparticle Random Phase Approximation (pn-QRPA). Extensive calculation of stellar weak interaction rates and associated gamma heating rates for 709 nuclei with $A = 18$ to 100, taking sd -shell nuclei with $A = 18-39$ and $Z = 10-20$ as first phase of the project, using the pn-QRPA theory was carried out by Nabi and Klapdor (Nabi & Klapdor-Kleingrothaus 1999; Nabi & Klapdor-Kleingrothaus 2004). In addition, these calculations also included neutrino cooling rates, β -delayed proton(neutron) emissions probabilities and energy rates of proton(neutron) emissions. In later works, these rates were calculated by using latest experimental data, fine tuning of the model parameters and

refined algorithms (Nabi & Klapdor-Kleingrothaus 1999a)-(J. -U. Nabi 2008). In subsequent papers (see (Nabi & Rahman 2007), (J. -U. Nabi 2008a) and (J. -U. Nabi 2008)) the authors calculated the Gamow-Teller transitions, the electron capture rates and neutrino cooling rates for ^{24}Mg .

In the current work, for the sake of direct comparison, we use the same density and temperature range and grid points as found in earlier works on heating and cooling rates for sd -shell nuclei (Oda et al. 1994) and (Takahara et al. 1989) who used a range as narrow as ($9.00 \leq \log \rho Y_e (\text{g cm}^{-3}) \leq 11.00$) and ($8.20 \leq \log T(K) \leq 9.60$). These authors have calculated these rates for sd -shell nuclei in full shell model configuration using effective interaction of Wildenthal (Wildenthal 1984). Other computational works on electron capture and β -decay rates in this connection by (Martínez-Pinedo et al. 2014) using large scale shell model (LSSM) and by (Suzuki et al. 2016), using the shell-model calculation in sd -shell with USDB Hamiltonian are also worth mentioning. The neutrino cooling rates in URCA pair with $A=23$ and 25 are crucial to determine the cooling rate of O-Ne-Mg core. In contrast, nuclei with $A=20$ and 24 are the key species for the core-contraction and heat generation rates in the core (Suzuki et al. 2016).

Our present work is devoted to a detailed analysis of the neutrino cooling and gamma heating rates due to weak-interaction reactions on sd -shell nuclei in stellar environment. The current work employs recent values of physical constants, mass data and model input parameters as compared to the earlier work of (Nabi & Klapdor-Kleingrothaus 1999). In addition we calculate neutrino cooling and gamma heating rates for nuclei with $Z = 8$ and 9 (not calculated in (Nabi & Klapdor-Kleingrothaus 1999)). The calculated rates can be associated with four different weak-interaction processes i.e. the β^\pm -decay and electron and positron captures. It is to be noted that there can be a fifth mode in which all parent excited states decay to ground state through gamma transition when $E_i \leq S_n$ or S_p (not included in this work).

In Section 2, we present the briefs of formalism for electron capture and β -decay rates as well as neutrino cooling and γ -ray heating rates. In Section 3, we discuss the results and compare them with previous works. These include the earlier pn-QRPA calculation (Nabi & Klapdor-Kleingrothaus 1999) and shell model calculations (Oda et al. 1994) and (Suzuki et al. 2016). The summary and conclusions are given in Section 4.

2 Model Description and Formalism

In this section, a brief description of the pn-QRPA model is presented. To save space the detailed model formalism is not reproduced here, for which we refer to (Nabi & Klapdor-Kleingrothaus 1999).

2.1 Hamiltonian and model parameters:

The Hamiltonian of the pn-QRPA model is given by

$$H^{QRPA} = H^{sp} + V^{pair} + V_{GT}^{ph} + V_{GT}^{pp}. \quad (1)$$

Wave functions and single particle energies were calculated using the Nilsson model (axially deformed). Pairing in nuclei was treated within the BCS approximation. The proton-neutron residual interaction occurs through particle-particle (pp) and particle-hole (ph) channels. In pn-QRPA, these interaction (force) terms were given a separable form as V_{GT}^{ph} for the particle-hole Gamow-Teller force denoted by model parameter χ and V_{GT}^{pp} for the particle-particle Gamow-Teller force denoted by model parameter κ . In this work, the values of χ and κ were optimized to produce terrestrial half lives with a percent deviation range of about 10%. These values of χ and κ resulted in fulfillment of Ikeda Sum Rule which we discuss later.

Creation operators of QRPA phonons are defined by

$$A_\omega^\dagger(\mu) = \sum_{pn} [X_\omega^{pn}(\mu) a_p^\dagger a_n^\dagger - Y_\omega^{pn}(\mu) a_n a_{\bar{p}}]. \quad (2)$$

In Eq. 2, $(a_{p(n)}^\dagger, a_{p(n)})$ forms a quasi-particle (q.p.) basis using Bogoliubov transformation (\bar{p} represents time-reversed state of p), indices p and n denote $m_p \alpha_p$ and $m_n \alpha_n$, respectively, and differentiate between proton and neutron single-(quasi)-particle states. The sum runs over proton-neutron pairs which satisfy $\mu = m_p - m_n$ and $\pi_p \pi_n = 1$, with π being parity, m specifies the Nilsson eigenstates and α represents additional quantum numbers.

For the separable forces, the pn-QRPA matrix equation can be articulated more clearly as

$$X_\omega^{pn} = \frac{1}{\omega - \varepsilon_{pn}} [2\chi(q_{pn} Z_\omega^- + q_{pn}^* Z_\omega^+) - 2\kappa(q_{pn}^U Z_\omega^{--} + q_{pn}^V Z_\omega^{++})], \quad (3)$$

$$Y_\omega^{pn} = \frac{1}{\omega + \varepsilon_{pn}} [2\chi(q_{pn} Z_\omega^+ + q_{pn}^* Z_\omega^-) + 2\kappa(q_{pn}^U Z_\omega^{++} + q_{pn}^V Z_\omega^{--})], \quad (4)$$

where $\varepsilon_{pn} = \varepsilon_p + \varepsilon_n$ (quasiparticle energies determined from a BCS calculation),

$$\begin{aligned} q_{pn} &= f_{pn} u_p v_n, \quad q_{pn}^U = f_{pn} u_p u_n, \\ \tilde{q}_{pn} &= f_{pn} v_p u_n, \quad q_{pn}^V = f_{pn} v_p v_n, \end{aligned}$$

with

$$f_{pn}(\mu) = \sum_{j_p j_n} D_{j_p}^{m_p \alpha_p} D_{j_n}^{m_n \alpha_n} \langle j_p m_p | t - \sigma_\mu | j_n m_n \rangle, \quad (5)$$

as the single-particle GT transition amplitudes defined in the Nilsson basis. D is the transformation matrix constructed from the Nilsson eigenfunctions.

$$Z_\omega^- = \sum_{pn} (X_\omega^{pn} q_{pn} - Y_\omega^{pn} \tilde{q}_{pn}) \quad (6)$$

$$Z_\omega^+ = \sum_{pn} (X_\omega^{pn} \tilde{q}_{pn} - Y_\omega^{pn} q_{pn}) \quad (7)$$

$$Z_\omega^{--} = \sum_{pn} (X_\omega^{pn} q_{pn}^U + Y_\omega^{pn} q_{pn}^V) \quad (8)$$

$$Z_\omega^{++} = \sum_{pn} (X_\omega^{pn} q_{pn}^V + Y_\omega^{pn} q_{pn}^U). \quad (9)$$

Using the normalization condition of the phonon amplitudes

$$\sum_{pn} [(X_\omega^{pn})^2 - (Y_\omega^{pn})^2] = 1, \quad (10)$$

the absolute values were determined by inserting Z'_ω 's into Eq. 3 and Eq. 4.

GT transition amplitudes from the QRPA ground state $|-\rangle$ (QRPA vacuum; $A_\omega(\mu)|-\rangle = 0$) to one-phonon states $|\omega, \mu\rangle = A_\omega^\dagger(\mu)|-\rangle$ were calculated as

$$\langle \omega, \mu | \sigma_\mu \tau_\pm | - \rangle = \mp Z_\omega^\pm. \quad (11)$$

Excitation energies of the one-phonon states are given by $\omega - (\varepsilon_p + \varepsilon_n)$, where ε_p and ε_n are energies of the single q.p. states of the smallest q.p. energy in the proton and neutron systems, respectively.

The RPA equation was solved for excitations from the $J^\pi = 0^+$ ground state of an even-even nucleus. In the present model, excited states of even-even nuclei were obtained by one-proton (or one-neutron) excitations. They were described, in the q.p. picture, by adding two-proton (two-neutron) q.p.'s to the ground state (Muto et al. 1992). Transitions from these initial states were then possible to final proton-neutron q.p. pair states in the odd-odd daughter nucleus. The

transition amplitudes and their reduction to correlated (c) one-q.p. states are given by

$$\begin{aligned} & \langle p^f n_c^f | \sigma_{-\mu} \tau_\pm | p_1^i p_{2c}^i \rangle \\ &= -\delta(p^f, p_2^i) \langle n_c^f | \sigma_{-\mu} \tau_\pm | p_{1c}^i \rangle \\ & \quad + \delta(p^f, p_1^i) \langle n_c^f | \sigma_{-\mu} \tau_\pm | p_{2c}^i \rangle \quad (12) \\ & \langle p^f n_c^f | \sigma_\mu \tau_\pm | n_1^i n_{2c}^i \rangle \\ &= +\delta(n^f, n_2^i) \langle p_c^f | \sigma_\mu \tau_\pm | n_{1c}^i \rangle \\ & \quad - \delta(n^f, n_1^i) \langle p_c^f | \sigma_\mu \tau_\pm | n_{2c}^i \rangle \end{aligned}$$

where $\mu = -1, 0, 1$, are the spherical components of the spin operator. For the construction of odd-A and odd-odd nuclei we refer to (Muto et al. 1992).

Ikeda Sum Rule (Ikeda 1964) is a mathematical tool which connects the nucleon numbers (neutrons and protons) with the microscopic structure of a given nucleus through the total Gamow Teller strengths in either direction. It is formulated as:

$$S^+ - S^- = \sum_f \langle f | \sigma \tau_- | i \rangle^2 - \sum_f \langle f | \sigma \tau_+ | i \rangle^2 = 3(N - Z) \quad (13)$$

This rule is model independent and provides a guideline for all theoretical calculations of GT strength function. Theoretical calculations of GT strength functions are supposed to fulfill the Ikeda sum rule. In our model the Hamiltonian (Eq. 1) was tuned to reproduce the Ikeda sum rule. In other words the daughter spectrum was forced not to have a deficit of GT strength value.

The other requisite parameters for calculation of weak rates and associated neutrino cooling and gamma ray heating rates are the Nilsson potential parameters, the pairing gaps, the nuclear quadrupole deformation, and the Q-values of the reactions. Nilsson-potential parameters were adopted from Ref. (Nilsson 1955) and the Nilsson oscillator constant was chosen as $\hbar\omega = 41A^{-1/3}(MeV)$ (the same for protons and neutrons). The relation for pairing gaps used in the present work is given as: $\Delta_p = \Delta_n = 12/\sqrt{A}(MeV)$. Nuclear quadrupole deformation parameter play a significant role in the pn-QRPA calculation, as argued by (Staudt et al. 1990) and later by (Nabi & Boyukata 2017). Measured (or theoretically predicted) values for the deformation parameter β were taken from (Raman et al. 2001). Here the authors estimated the β parameter, for even-even isotopes, by relating reduced electric quadrupole transition probability, $B(E2)\uparrow$ with the quadrupole deformation as:

$$\beta = \frac{4\pi}{3ZR_0^2} [B(E2)\uparrow / e^2]^{1/2} \quad (14)$$

where Z and A are the atomic and mass numbers, respectively, and $R_0^2 = 0.0144A^{2/3}$ barn. For remaining cases (non even-even), the electric quadrupole deformation values were taken from Möller and collaborators (Möller et al. 2016). Q-values were taken from the recent mass compilation of Wang and collaborators (Wang et al. 2012). Using these new compilations and a model space of $5\hbar\omega$, we calculated neutrino cooling and gamma ray heating rates associated with weak interaction processes in astrophysical environments.

2.2 The Rates Formalism:

The basic formalism for calculation of stellar weak rates was adopted from the pioneering work of Fuller, Fowler and Newman (Fuller et al. 1980, 1982,a, 1985). However it is to be noted that, unlike the work of Fuller, Fowler and Newman, we calculated all GT strength distributions from parent excited states in a microscopic fashion.

The weak decay rate from the i th state (parent nucleus) to the j th state (daughter nucleus) is given by

$$\lambda_{ij} = \left(\frac{\ln 2}{D}\right) [\phi_{ij}(T, \rho, E_f)][B(F)_{ij} + (g_A/g_V)^2 B(GT)_{ij}]. \quad (15)$$

The value of D was taken to be 6143s (Hardy et al. 2009). $B(F)_{ij}$ denote the total reduced transition probabilities due to Fermi interaction and $B(GT)_{ij}$ due to Gamow-Teller interactions. The value of (g_A/g_V) , denoting the ratio of axial and vector coupling constants, was taken as -1.2694 (Nakamura et al. 2010). The ϕ_{ij} are the phase space integrals and are functions of stellar temperature (T), density (ρ) and Fermi energy (E_f) of the electrons. The phase space integrals were separately calculated using the relation (we use natural units in this section, $\hbar = m_e = c = 1$):

$$\phi_{ij} = \int_1^{w_m} w \sqrt{w^2 - 1} (w_m - w)^2 F(\pm Z, w) (1 - D_{\mp}) dw, \quad (16)$$

whereas the phase space for continuum positron (*lower signs*) or electron (*upper signs*) capture was calculated using:

$$\phi_{ij} = \int_{w_l}^{\infty} w \sqrt{w^2 - 1} (w_m + w)^2 F(\pm Z, w) D_{\mp} dw. \quad (17)$$

In Eqs. (16) and (17) w is the total energy (rest+kinetic) of the electron or positron, w_l is the total threshold energy (rest+kinetic) for positron (or electron) capture. $F(\pm Z, w)$ are the Fermi functions and

were calculated according to the procedure adopted by (Gove and Martin 1971). Finite nuclear size corrections as well as screening corrections were undertaken within the recipe adopted by (Gove and Martin 1971). D_{\pm} is the Fermi-Dirac distribution function for positrons (electrons).

$$D_{+} = \left[\exp \left(\frac{E + 2 + E_f}{kT} \right) + 1 \right]^{-1}, \quad (18)$$

$$D_{-} = \left[\exp \left(\frac{E - E_f}{kT} \right) + 1 \right]^{-1}, \quad (19)$$

where E is the kinetic energy of the electrons and k is the Boltzmann constant.

The number density of protons associated with electrons and nuclei is $\rho Y_e N_A$, where ρ is the baryon density, Y_e is the ratio of electron number to the baryon number, and N_A is the Avogadro number.

$$\rho Y_e = \frac{1}{\pi^2 N_A} \left(\frac{m_e c}{\hbar} \right)^3 \int_0^{\infty} (D_{-} - D_{+}) p^2 dp, \quad (20)$$

where $p = (w^2 - 1)^{1/2}$ is electron's momentum, and Eq. 20 has units of *moles cm⁻³*. This equation was used for an iterative calculation of Fermi energies for selected values of ρY_e and T .

The calculation of neutrino and antineutrino cooling rates was carried out by using the following equations:

$$\lambda_{ij}^{\nu(\bar{\nu})} = \left(\frac{\ln 2}{D}\right) [\phi_{ij}^{\nu}(T, \rho, E_f)][B(F)_{ij} + (g_A/g_V)^2 B(GT)_{ij}]. \quad (21)$$

where all the constants and variables have their usual meaning as discussed earlier in Eq. (15). The ϕ_{ij}^{ν} are the phase space integrals and are functions of stellar temperature (T), density (ρ) and Fermi energy (E_f) of the electrons. They are explicitly given by

$$\phi_{ij}^{\nu} = \int_1^{w_m} w \sqrt{w^2 - 1} (w_m - w)^3 F(\pm Z, w) (1 - D_{\mp}) dw, \quad (22)$$

and by

$$\phi_{ij}^{\nu} = \int_{w_l}^{\infty} w \sqrt{w^2 - 1} (w_m + w)^3 F(\pm Z, w) D_{\mp} dw. \quad (23)$$

All symbols have meanings as discussed earlier. For details on calculation of reduced transition probabilities we refer to (Nabi& Klapdor-Kleingrothaus 2004). The total neutrino cooling rate per unit time per nucleus is given by

$$\lambda^{\nu} = \sum_{ij} P_i \lambda_{ij}^{\nu}, \quad (24)$$

where λ_{ij}^ν is the sum of the electron capture and positron decay rates for the transition $i \rightarrow j$.

The total gamma ray heating rates for a given nuclear specie are given by:

$$\lambda^\gamma = \sum_{ij} P_i \lambda_{ij} E_j, \quad (25)$$

where P_i , in Eqs. (24) and (25), denotes the probability of occupation of parent excited states and follows the Boltzmann statistical distribution, λ_{ij} gives the sum of the electron capture and positron decay rates, $\lambda_{ij} = \lambda_{ij}^{ec} + \lambda_{ij}^{pd}$, or the sum of positron capture and electron decay rates, $\lambda_{ij} = \lambda_{ij}^{pc} + \lambda_{ij}^{ed}$, for the transition $i \rightarrow j$ and E_j is the energy of daughter's excited state.

3 Results and Discussion

Our calculated $B(GT)$ strength for even-even and odd- A nuclei are shown in Figs. (1 - 2). Fig. 1 shows the pn-QRPA calculated $B(GT)$ strength for even-even oxygen isotopes along the β -decay direction. We also compare our calculated GT strength with the shell model results of (Oda et al. 1994). For odd- A nuclei we calculated our $B(GT)$ strength values along electron capture direction for ^{23}Na and ^{25}Mg and compared with the shell model calculation of (Suzuki et al. 2016) (see Fig. 2). Authors in (Suzuki et al. 2016) calculated GT strength distribution only till 10 MeV in daughter nuclei. We also present our calculated $B(GT)$ strength distribution only up to excitation energy of 10 MeV in Fig. 2. The comparison of total GT strength and centroid values of data shown in Figs (1 - 2) is given in Table 1. It may be seen from Table 1 that our model calculates bigger total GT strength and low residing centroid values for even-even nuclei when compared with the shell model results. The comparison is interesting for odd- A nuclei. The calculated GT strength distributions later directly affect the computed weak rates in stellar matter.

The γ -ray heating rates due to $A=20$ nuclei are shown in Fig. 3, the left hand panel shows these rates in electron capture direction and right hand panel in β -decay direction. We see that with exception of ^{20}O , where both rates are nearly equal, the other nuclei like ^{20}F , ^{20}Ne and ^{20}Na have enhanced gamma heating rates due to electron capture reactions. Specially, at high densities there is an orders of magnitude increase in the gamma ray heating rates due to electron capture. A similar trend may be seen for ^{25}Mg and ^{25}Na in Fig. 4.

The neutrino and antineutrino cooling rates due to weak rates on $A=24$ nuclei can be seen in Fig. 5. Here

we have plotted the rates for only ^{24}Ne , ^{24}Na and ^{24}Mg at selected densities. Logically, the neutrino cooling rates are orders of magnitude more efficient than the corresponding antineutrino rates, though both escape the core without attenuation and tend to cool the core. Fig. 6 shows the neutrino and antineutrino cooling rates due to $A=25$ nuclei. For ^{25}Na and ^{25}Mg , a similar trend is witnessed for the cooling rates.

We display our calculated heating and cooling rates for selected sd shell nuclei in Tables (2 - 8). Table 2 shows the associated gamma ray heating rates and Table 3 the associated neutrino (antineutrino) cooling rates for ^{20}O , ^{20}F , ^{20}Na and ^{20}Ne , respectively, as a function of stellar temperature and density. Table 4 and Table 5 show results for ^{23}O , ^{23}F , ^{23}Ne , ^{23}Na and ^{23}Mg in a similar format. Table 6 and Table 7 enlist the gamma ray heating rates and neutrino cooling rates for $A=24$ nuclear species, respectively. Table 8 shows the pn-QRPA calculated heating and cooling rates for ^{25}Na and ^{25}Mg . From these tables, it can be concluded, that the gamma ray heating and neutrino cooling rates, due to both electron capture and β -decay on sd shell nuclei, increase with increasing core temperature. This is because of a corresponding increment in the electron capture and β -decay rates on these nuclei with increasing stellar temperature. The β -decay rates decrease with increasing stellar density (because of increase in Fermi energy and decrease in phase space factor). Accordingly we note that the heating rate along β -decay direction decreases with increasing density. A similar explanation follows for the neutrino cooling rates. We note that the heating and cooling rates play a dominant role in the stellar core evolution of $8\text{-}10 M_\odot$ stars. The ASCII files of all calculated heating and cooling rates are available and may be requested from corresponding author to be used in simulation codes.

We compare our current calculation with previous published work of (Nabi & Klapdor-Kleingrothaus 1999)(referred to as ADNDT99) using the same theory. We also compare our work with previous shell model calculations: (Oda et al. 1994) (referred to as OHMTS) and (Suzuki et al. 2016) (referred to as STN16). It is to be noted that the shell model calculation of STN16 includes the effects of Coulomb corrections while those of OHMTS do not. The electron capture, neutrino cooling and gamma heating rates are generally smaller for STN16 when compared with OHMTS rates. We also incorporated Coulomb corrections in our calculation.

The mutual comparison may be seen in Tables (9 - 10) for $A = 23$ and Tables (11 - 12) for $A = 25$. For the comparison we selected the pairs $^{23}\text{Na} \rightarrow ^{23}\text{Ne}$, $^{23}\text{Ne} \rightarrow ^{23}\text{F}$ and $^{25}\text{Mg} \rightarrow ^{25}\text{Na}$, $^{25}\text{Na} \rightarrow ^{25}\text{Ne}$. All these tables

are shown in the electron capture direction. In these tables the right hand column (group of four sub columns) enlists the respective neutrino cooling rates and a similar column on the left hand shows the gamma ray heating rates in each table.

Comparing the current gamma heating rates due to electron capture rates on ^{23}Na with ADNDT99 rates (Table 9), we note that current rates are up to an order of magnitude bigger at high temperatures. The new gamma heating rates are in better comparison with shell model rates, specially at high temperatures and densities. For density range $10^{10} - 10^{11}$ (g.cm $^{-3}$) the comparison is fair albeit the shell model rates are factor 3–8 bigger. At $T_9 = 30$, the shell model rates are factor 3–4 bigger. The new calculated neutrino cooling rates, on the other hand, are generally in better agreement with shell model rates.

Table 10 shows that the new pn-QRPA calculated gamma heating rates, due to electron capture on ^{23}Ne , are up to an order of magnitude bigger compared with ADNDT99 rates. The comparison with ADNDT99 rates improves as stellar core stiffens to high densities. It is noted that at low temperatures, $T_9 = 0.01\text{--}0.1$, shell model gamma heating rates are many orders of magnitude smaller than pn-QRPA rates. Only at density 10^{11} (g.cm $^{-3}$) are the two rates in good agreement. This is because the pn-QRPA model incorporated particle emission processes in their calculation not considered in shell model calculations. In the pn-QRPA calculation all excited states, with energy less than separation energy of neutron (proton) decay directly to ground state via γ transitions. At high temperatures $T_9 = 30$, our rates are in very good agreement with shell model rates. The pn-QRPA calculated neutrino cooling rates are up to an order of magnitude bigger than shell model rates.

The pn-QRPA calculated gamma heating rates, due to electron capture on ^{25}Mg , are in decent agreement with shell model rates for high densities $10^{10} - 10^{11}$ (g.cm $^{-3}$), as can be seen from Table 11. For smaller density range the shell model heating rates are orders of magnitude bigger (specially at low temperatures). Our neutrino cooling rates are an order of magnitude bigger than shell model rates. However at $T_9 = 30$, the pn-QRPA and shell model rates are in good agreement.

Table 12 shows that our gamma heating rates, due to electron capture on ^{25}Na , are in good concordance with shell model rates for high densities $10^{10} - 10^{11}$ (g.cm $^{-3}$). Contrary to Table 11, at low temperatures and densities the pn-QRPA gamma heating rates are orders of magnitude bigger than shell model heating rates. The neutrino cooling rates are again an order of magnitude bigger than shell model rates.

Finally we present the comparison of gamma heating and neutrino cooling rates for a sample even-even nucleus. Table 13 compares the gamma heating and neutrino cooling rates due to β^- -decay from ^{20}O . It is again noted that (Nabi & Klapdor-Kleingrothaus 1999) did not calculate weak rates for nuclei with $Z < 10$ and as such we compare our calculation with the shell model calculations of OHMTS and STN16. A very decent comparison between pn-QRPA and shell model calculations is noted for the gamma heating rates due to β -decay from ^{20}O . Only at $T_9 = 30$ are the shell model rates factor four bigger. OHMTS also considered transitions from excited states much higher than the lesser of the S_p or S_n values, which causes their rates to increase at higher temperatures. We argue that such contributions should not be considered. At any E_i higher than the lesser of S_p or S_n (after accounting for the effective Coulomb barrier hindering the emission of prompt protons and for the uncertainty in the calculation of energy levels), the nucleus will emit protons or neutrons instead of continuing to undergo β -decay. On the other hand the pn-QRPA calculated neutrino cooling rates are orders of magnitude smaller, specially at low temperatures. At $T_9 = 30$, the pn-QRPA cooling rates are an order of magnitude smaller. It should be pointed out that the rates are sensitive functions of the difference of parent and daughter energies ($E_i - E_j$) and just by a mere addition of around 0.5 MeV, many of our small rates could increase by orders of magnitude.

To summarize the comparison of current work with previous calculations, it can be noted that the new pn-QRPA rates are up to an order of magnitude bigger than ADNDT99 rates. This we attribute to optimal choice of model parameters and use of latest values of mass defect and physical constants. Shell model rates are generally in excellent agreement with our calculation at high temperatures. At low temperatures and densities, orders of magnitude difference is witnessed. This is due to multiple effects. Firstly shell model did not take into account particle emission processes from parent excited states. The calculation of energy eigenvalues in the two models may contribute to the differences in the total rates (see Eqs. (24) and (25)). But also the calculation of total GT strength values and placement of GT centroids, in the two models, resulted in this difference. The pn-QRPA model generally favors cooler cores due to bigger cooling rates (see also discussion in (Nabi & Klapdor-Kleingrothaus 1999)). It is now left to the simulators to analyze these differences and check whether their prediction makes the core evolve towards ECSN, CCSN or any other interesting occurrence.

4 Conclusions

Semi-leptonic weak-interaction mediated rates for nuclei in stellar core are important factors in determining the thermodynamic and hydrodynamic trajectories of stars in the late stages of their evolution. The outcome of rapid contraction of electron-degenerate O-Ne-Mg cores of $8\text{-}10 M_{\odot}$ stars is determined by contraction, heating and cooling processes in the stellar core. All these processes compete with one another. Result of these competitive processes decide whether the star would end up its life as a core-collapse or electron capture supernova. In this work we presented gamma ray heating and (anti)neutrino cooling rates due to electron capture and β -decays on *sd*-shell nuclei in stellar environment. The cooling rates are important for the $A = 23$ and 25 nuclei for nuclear URCA process. On the other hand $A = 20$ and 24 nuclei rates are significant for heat generation and core-contraction rates in the O-Ne-Mg cores.

For our calculation we used the pn-QRPA in a multi-shell deformed single-particle space with a schematic separable interaction to calculate gamma heating and (anti)neutrino cooling rates due to weak rates on key *sd*-shell nuclei. An optimum choice of model parameters and incorporation of recent experimental mass compilation resulted in a reliable calculation of Gamow-Teller strength distributions that fulfilled the model-independent Ikeda sum rule. The cooling and heating rates were calculated for density range ($10 \leq \rho(\text{g.cm}^{-3}) \leq 10^{11}$) and temperature range ($0.01 \times 10^9 \leq T(K) \leq 30 \times 10^9$). The calculated rates were compared with previous pn-QRPA calculation (ADNDT99) as well as previous shell model rates (OHMTS and STN16) and interesting differences were reported.

The pn-QRPA calculated gamma heating rates are generally bigger than those calculated by shell model rates. ^{25}Mg was the only exception where at density range $10^7 - 10^9 (\text{g.cm}^{-3})$ the shell model heating rates were orders of magnitude bigger. At high temperatures the shell model and pn-QRPA gamma heating rates are in reasonable agreement. At times the shell model rates are slightly bigger and sometimes the pn-QRPA heating rates are marginally bigger. The neutrino cooling rates calculated using the pn-QRPA model is up to an order of magnitude bigger compared with shell model rates for the $A = 23$ and 25 nuclei (odd- A cases). The implications of these cooling and heating rates worth attention of core-collapse simulators. They are urged to test-run our calculated rates to see whether the stars end up as a white dwarf, an ECSN or CCSN.

Acknowledgements The authors would like to acknowledge the assistance of the anonymous referee

which led to a substantial improvement of the paper. J.-U. Nabi would like to acknowledge the support of the Higher Education Commission Pakistan through the HEC Projects No. 20-3099 and 5557/KPK/NRPU/R&D/HEC/2016.■

References

- M. Wang, G. Audi, A.H. Wapstra, F.G. Kondev, M. MacCormick, X. Xu, and B. Pfeiffer B, Chin. Phys. C **36** (2012) 1603.
- P. Möller A. J. Sierk, T. Ichikawa, and H. Sagawa, At. Data Nucl. Data Tables **109** (2016) 1-204.
- S. Raman, C. W. Nestor, and P. Tikkanen. At. Data Nucl. Data Tables **78(1)** (2001) 1-128.
- S. E. Woosley, A. Heger, and T. A. Weaver, Rev. Mod. Phys. **74** (2002) 1015.
- M. Halabi, Ghina, and Mounib El Eid. AIP Conf. Proc. **1645(1)** (2015) 339-343.
- S. G. Ryan, A. J. Norton, Stellar Evolution and Nucleosynthesis. Cambridge University Press. (2010) 135-136. ISBN 978-0-521-13320-3.
- S. Miyaji, K. Nomoto,K. Yokoi, and D. Sugimoto, Publ. Astron. Soc. Japan **32**, (1980) 303.
- S. E. Woosley, and T. A. Weaver, Astrophys. J. **238** (1980) 1017-1025.
- K. Nomoto Astrophys. J. **322** (1987) 206-214.
- J. Gutiérrez, R. Canal, and E. García-Berro. Astron. & Astrophys. **435(1)** (2005) 231-237.
- S. Miyaji, and K. Nomoto, Astrophys. J. **318** (1987) 307-315.
- M. Takahara, M. Hino, T. Oda, K. Muto, A. A. Wolters, P. W. M. Glaudemans, and K. Sato, Nucl. Phys. A **504(1)** (1989) 167-192.
- B. H. Wildenthal. Prog. Part. Nucl. Phy., edited by D. H. Wilkinson (Pergamon, Oxford) **11** (1984) 5.
- B. A. Brown and W. A. Richter, Phys. Rev. C **74** (2006) 034315.
- W. A. Richter, S. Mkhize, and B. A. Brown, Phys. Rev. C **78** (2008) 064302.
- E. García-Berro, C. Ritossa and I. Iben, Astrophys. J. **485(2)** (1997) 765
- S. Gupta, E. F. Brown, H. Schatz, P. Möller, and K. -L. Kratz, Astrophys. J. **662(2)** (2007) 1188.
- S. Jones, R. Hirschi, K.I. Nomoto, T. Fischer, F.X. Timmes, F. Herwig, B. Paxton, H. Toki, T. Suzuki, G. Martinez-Pinedo, and Y.H.Lam, Astrophys. J. **772(2)** (2013) 150.
- G. Martínez-Pinedo, Y. H. Lam, K. Langanke, R. G. T. Zegers, and C. Sullivan, Phys. Rev. C **89(4)** (2014) 045806.
- T. Suzuki, H. Toki, and K. I. Nomoto, The Astrophy. J. **817(2)** (2016) 163.
- T. Oda, M. Hino, K. Muto, M. Takahara, and K. Sato, At. Data Nucl. Data Tables **56** (1994) 231-403.
- J.-U. Nabi and H.V. Klapdor-Kleingrothaus, At. Data Nucl. Data Tables **71** (1999) 149.
- J.-U. Nabi and H.V. Klapdor-Kleingrothaus, Eur. Phys. J. A **5** (1999) 337
- J.-U. Nabi and H.V. Klapdor-Kleingrothaus, At. Data Nucl. Data Tables **88** (2004) 237
- J.-U. Nabi, Physica Scripta **78(3)** (2008) 035201.
- J.-U. Nabi, Phys. Rev. C **78(4)** (2008) 045801.
- K. Muto, E. Bender, T. Oda and H. V. Klapdor, Z. Phys. A **341** (1992) 407.
- J.-U. Nabi and M.-U. Rahman, Phys. Rev. C **75(3)** (2007) 035803.
- J. -U. Nabi and M. Böyükata Astrophys. Space Sci. **362(1)** (2017) 9.
- A. Staudt, E. Bender, K. Muto and H.V. Klapdor-Kleingrothaus, At. Data Nucl. Data Tables **44** (1990) 79.
- K. Nakamura, and Particle Data Group, J. Phys. G: Nucl. and Part. Phys. **37(7A)** (2010) 075021.
- V. Rodin, A. Faessler, F. Simkovic, and P. Vogel, Czech. J. Phys. **56** (2006) 495.
- G. M. Fuller, W. A. Fowler, and M. J. Newman, Astrophys. J. Supp. Ser. **42** (1980) 447.
- G. M. Fuller, W. A. Fowler, and M. J. Newman, Astrophys. J. **252** (1982) 715.
- G. M. Fuller, W. A. Fowler, and M. J. Newman, Astrophys. J. Supp. Ser. **48** (1982) 279.
- G. M. Fuller, W. A. Fowler, and M. J. Newman, Astrophys. J. **293** (1985) 1.
- J. C. Hardy and I. S. Towner, Phys. Rev. C **79(5)** (2009) 055502.
- N. B. Gove and M. J. Martin, At. Data Nucl. Data Tables, **10** (1971) 205.
- S. G. Nilsson, Mat. Fys. Medd. Dan. Vid. Selsk **29** (1955) 16.
- M. Hirsch, A. Staudt, K. Muto, and H. V. Klapdor-Kliengrothaus, Nucl. Phys. A **535** (1991) 62.
- I. Ikeda, Prog. Theor. Phys., **31** (1964) 434.

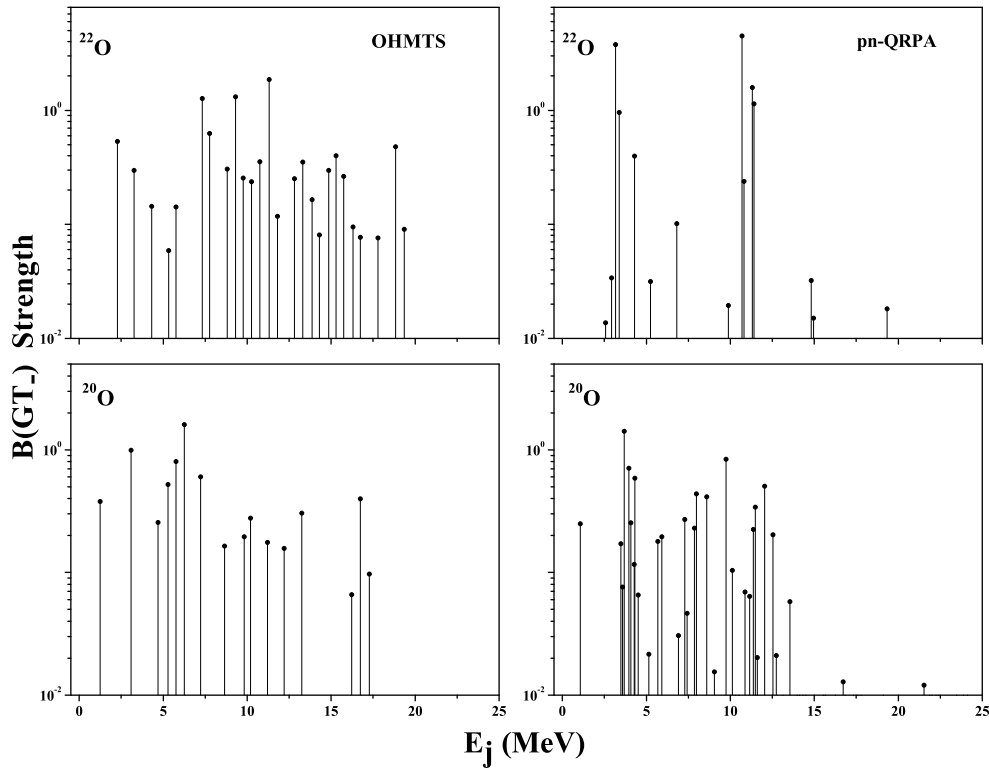


Fig. 1 Calculated $B(\text{GT})$ strength along β -decay direction for even-even oxygen isotopes. The left panels show the (Oda et al. 1994) calculation. Right panels show our calculated strength.

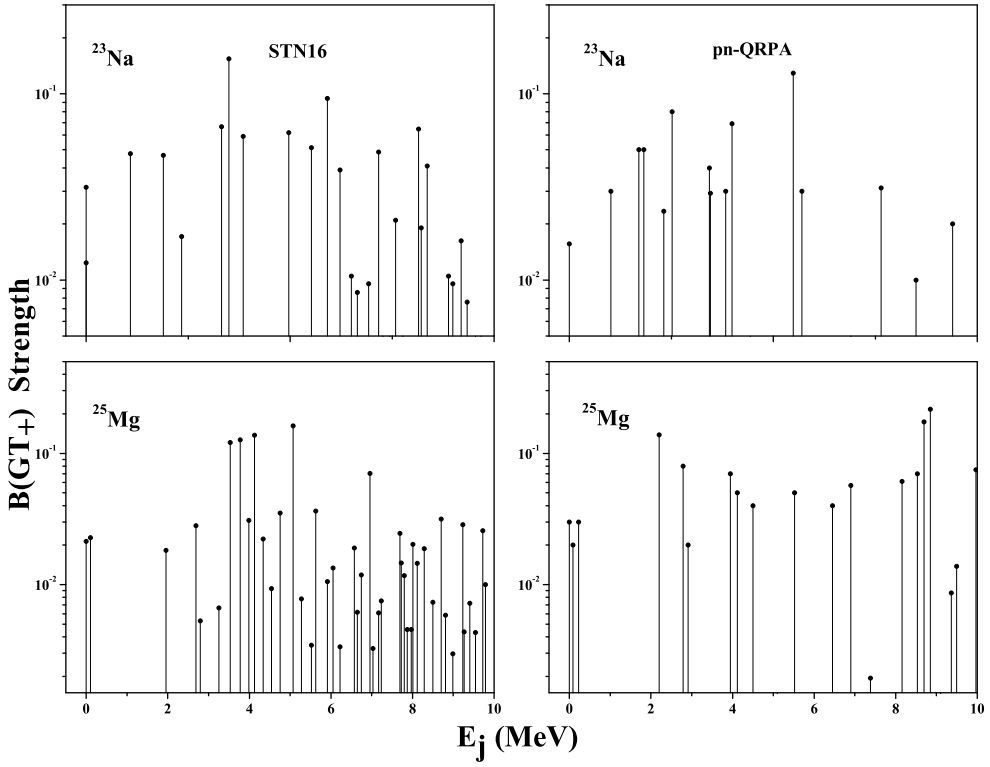


Fig. 2 Calculated $B(\text{GT})$ strength along electron capture direction for odd- A nuclei. The left panels show the (Suzuki et al. 2016) calculation. Right panels show our calculated strength.

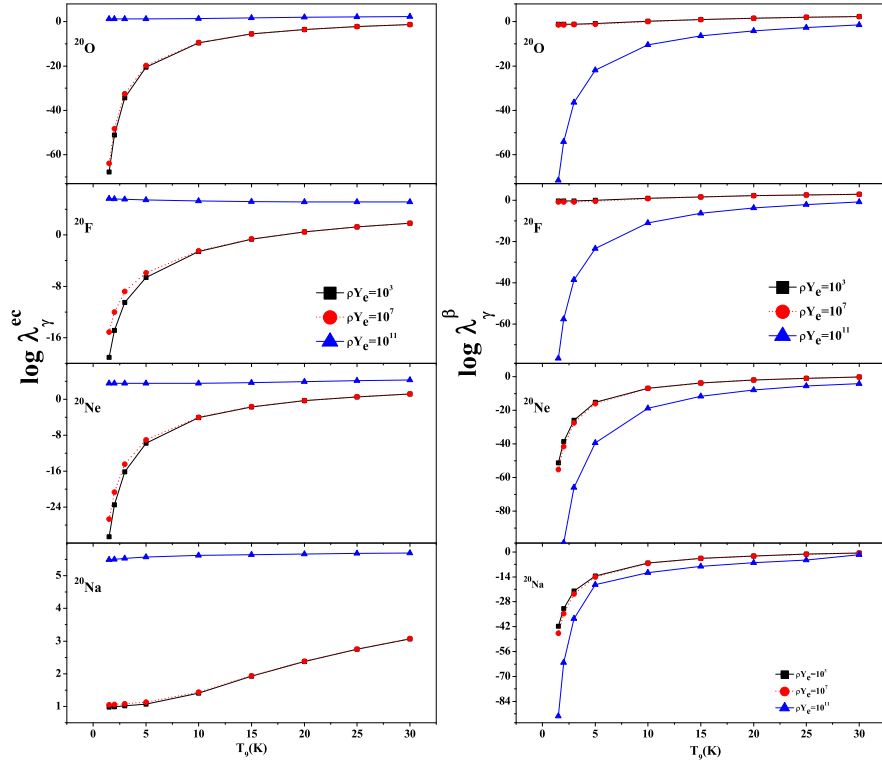


Fig. 3 Gamma ray heating rates due to β -decay and electron capture processes on $A = 20$ nuclei, at selected stellar densities ρY_e (g.cm^{-3}) and temperatures. T_9 gives the stellar temperature in units of 10^9 K.

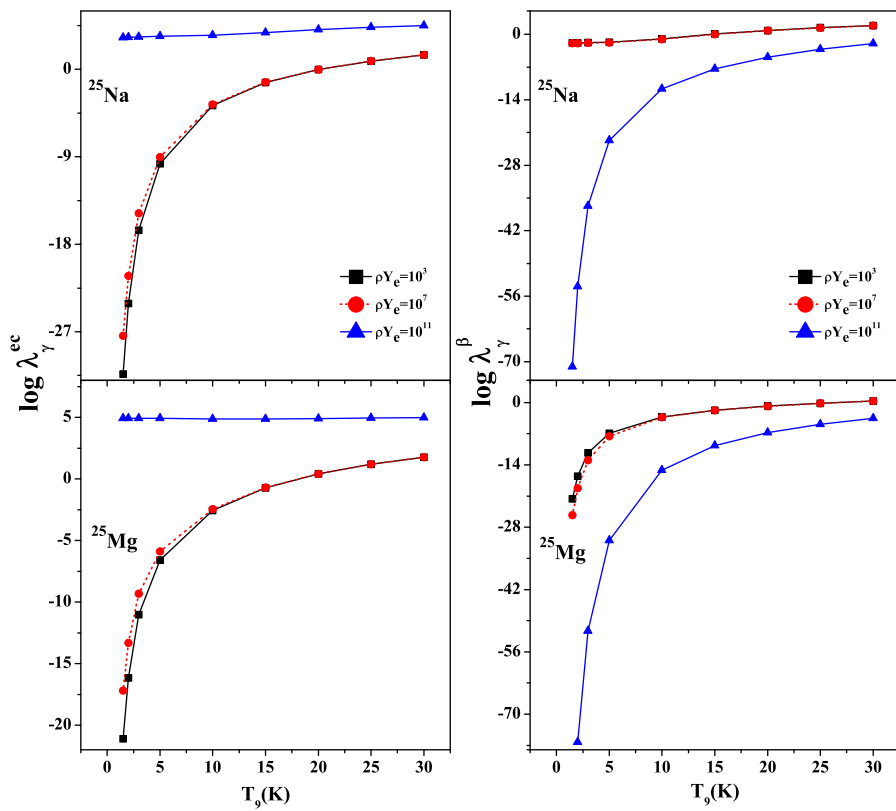


Fig. 4 Same as Fig. 3 but for $A = 25$ nuclei.

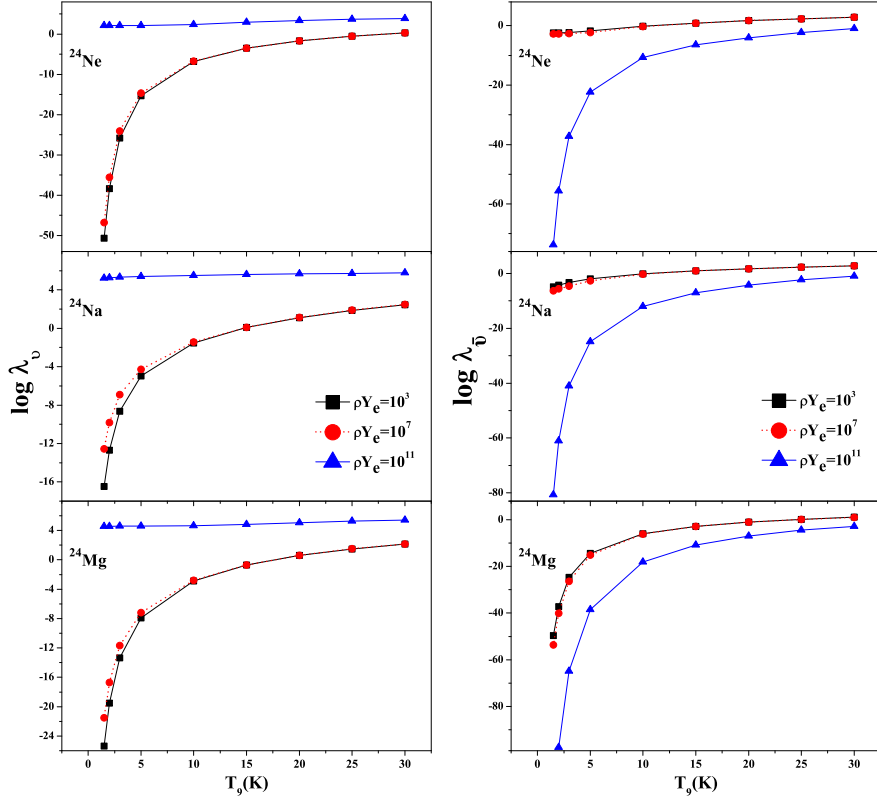


Fig. 5 Neutrino and antineutrino cooling rates due to β -decay and electron capture processes on $A = 24$ nuclei, at selected stellar densities ρY_e (g.cm^{-3}) and temperatures. T_9 gives the stellar temperature in units of 10^9 K.

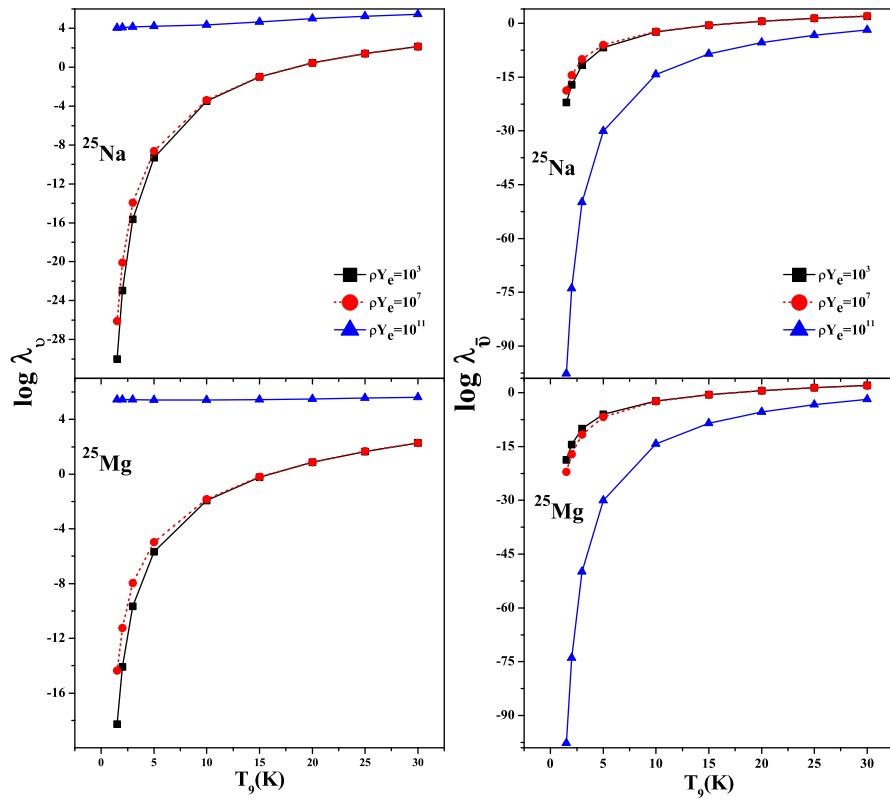


Fig. 6 Same as Fig. 5 but for $A = 25$ nuclei.

Table 1 Comparison of calculated total GT strength ($B(GT)_+$) and centroid (E_+) values, along electron capture direction, for ^{23}Na and ^{25}Mg and, along β -decay direction, for ^{20}O and ^{22}O .

Nuclei	$\sum B(GT)_+$		E_+ (MeV)	
	STN16	This Work	STN16	This Work
^{23}Na	0.964	0.64	4.99	3.90
^{25}Mg	1.19	1.25	5.25	6.16
$\sum B(GT)_-$		E_- (MeV)		
OHMTS	OHMTS	This Work	OHMTS	This Work
^{20}O	6.98	8.01	7.15	4.88
^{22}O	10.14	12.90	10.36	7.84

Table 2 Calculated γ -ray heating rates due to beta decay (λ_γ^β) and electron capture (λ_γ^{EC}) on ^{20}O , ^{20}F , ^{20}Ne and ^{20}Na at different selected densities and temperatures in stellar environment. The first column shows the stellar densities (ρY_e) (in units of g.cm $^{-3}$). The rates are tabulated in units of MeV.s $^{-1}$. In the table entry 1.00×10^{-100} means that calculated rate is smaller than 1.00×10^{-100} MeV.s $^{-1}$.

ρY_e (g.cm $^{-3}$)	T (K)	^{20}O		^{20}F		^{20}Ne		^{20}Na	
		λ_γ^β	λ_γ^{EC}	λ_γ^β	λ_γ^{EC}	λ_γ^β	λ_γ^{EC}	λ_γ^β	λ_γ^{EC}
10^1	1.00×10^7	6.14×10^{-2}	1.00×10^{-100}	4.13×10^{-1}	1.00×10^{-100}	1.00×10^{-100}	1.00×10^{-100}	1.00×10^{-100}	9.44×10^0
10^1	4.00×10^8	6.14×10^{-2}	1.00×10^{-100}	4.13×10^{-1}	6.22×10^{-60}	1.00×10^{-100}	1.00×10^{-100}	1.00×10^{-100}	9.44×10^0
10^1	7.00×10^8	6.14×10^{-2}	1.00×10^{-100}	4.13×10^{-1}	7.11×10^{-38}	1.00×10^{-100}	8.53×10^{-63}	1.72×10^{-87}	9.44×10^0
10^1	1.00×10^9	6.14×10^{-2}	1.00×10^{-100}	4.11×10^{-1}	7.31×10^{-28}	3.85×10^{-77}	3.05×10^{-45}	3.29×10^{-62}	9.44×10^0
10^1	2.00×10^9	6.19×10^{-2}	7.82×10^{-52}	3.93×10^{-1}	1.30×10^{-15}	2.54×10^{-39}	3.24×10^{-24}	1.30×10^{-32}	9.77×10^0
10^1	3.00×10^9	6.65×10^{-2}	5.38×10^{-35}	4.03×10^{-1}	3.06×10^{-11}	1.57×10^{-26}	7.48×10^{-17}	1.29×10^{-22}	1.04×10^1
10^1	5.00×10^9	1.19×10^{-1}	3.69×10^{-21}	7.89×10^{-1}	2.50×10^{-7}	5.28×10^{-16}	1.69×10^{-10}	3.66×10^{-14}	1.17×10^1
10^1	1.00×10^{10}	1.46×10^0	3.18×10^{-10}	7.98×10^0	2.61×10^{-3}	1.71×10^{-7}	8.38×10^{-5}	5.19×10^{-7}	2.52×10^1
10^1	1.50×10^{10}	9.59×10^0	2.70×10^{-6}	4.19×10^1	2.21×10^{-1}	2.44×10^{-4}	2.02×10^{-2}	2.28×10^{-4}	8.34×10^1
10^1	2.00×10^{10}	3.65×10^1	3.24×10^{-4}	1.44×10^2	3.05×10^0	1.19×10^{-2}	4.63×10^{-1}	6.27×10^{-3}	2.37×10^2
10^1	2.50×10^{10}	9.86×10^1	6.40×10^{-3}	3.78×10^2	1.79×10^1	1.35×10^{-1}	3.56×10^0	5.43×10^{-2}	5.62×10^2
10^1	3.00×10^{10}	2.16×10^2	5.01×10^{-2}	8.38×10^2	6.61×10^1	7.29×10^{-1}	1.52×10^1	2.58×10^{-1}	1.17×10^3
10^4	1.00×10^7	6.12×10^{-2}	1.00×10^{-100}	4.11×10^{-1}	1.00×10^{-100}	1.00×10^{-100}	1.00×10^{-100}	1.00×10^{-100}	9.44×10^0
10^4	4.00×10^8	6.12×10^{-2}	1.00×10^{-100}	4.12×10^{-1}	6.44×10^{-57}	1.00×10^{-100}	1.00×10^{-100}	1.00×10^{-100}	9.44×10^0
10^4	7.00×10^8	6.12×10^{-2}	1.00×10^{-100}	4.12×10^{-1}	1.66×10^{-35}	1.00×10^{-100}	1.99×10^{-60}	7.36×10^{-90}	9.44×10^0
10^4	1.00×10^9	6.12×10^{-2}	1.00×10^{-100}	4.11×10^{-1}	8.20×10^{-27}	3.43×10^{-78}	3.42×10^{-44}	2.93×10^{-63}	9.44×10^0
10^4	2.00×10^9	6.18×10^{-2}	7.87×10^{-52}	3.92×10^{-1}	1.41×10^{-15}	2.34×10^{-39}	3.52×10^{-24}	1.20×10^{-32}	9.77×10^0
10^4	3.00×10^9	6.65×10^{-2}	5.40×10^{-35}	4.02×10^{-1}	3.10×10^{-11}	1.55×10^{-26}	7.59×10^{-17}	1.27×10^{-22}	1.04×10^1
10^4	5.00×10^9	1.19×10^{-1}	3.69×10^{-21}	7.89×10^{-1}	2.51×10^{-7}	5.27×10^{-16}	1.69×10^{-10}	3.66×10^{-14}	1.17×10^1
10^4	1.00×10^{10}	1.46×10^0	3.18×10^{-10}	7.98×10^0	2.62×10^{-3}	1.71×10^{-7}	8.38×10^{-5}	5.19×10^{-7}	2.52×10^1
10^4	1.50×10^{10}	9.59×10^0	2.70×10^{-6}	4.20×10^1	2.21×10^{-1}	2.44×10^{-4}	2.02×10^{-2}	2.28×10^{-4}	8.34×10^1
10^4	2.00×10^{10}	3.66×10^1	3.24×10^{-4}	1.44×10^2	3.05×10^0	1.19×10^{-2}	4.65×10^{-1}	6.28×10^{-3}	2.37×10^2
10^4	2.50×10^{10}	9.89×10^1	6.41×10^{-3}	3.79×10^2	1.79×10^1	1.35×10^{-1}	3.57×10^0	5.45×10^{-2}	5.62×10^2
10^4	3.00×10^{10}	2.16×10^2	5.02×10^{-2}	8.38×10^2	6.62×10^1	7.31×10^{-1}	1.52×10^1	2.59×10^{-1}	1.17×10^3
10^7	1.00×10^7	3.69×10^{-2}	1.00×10^{-100}	9.27×10^{-2}	1.00×10^{-100}	1.00×10^{-100}	1.00×10^{-100}	1.00×10^{-100}	1.10×10^1
10^7	4.00×10^8	3.71×10^{-2}	1.00×10^{-100}	9.62×10^{-2}	3.72×10^{-47}	1.00×10^{-100}	5.53×10^{-91}	1.00×10^{-100}	1.10×10^1
10^7	7.00×10^8	3.74×10^{-2}	1.00×10^{-100}	1.02×10^{-1}	3.31×10^{-29}	1.00×10^{-100}	3.97×10^{-54}	3.69×10^{-96}	1.10×10^1
10^7	1.00×10^9	3.79×10^{-2}	2.47×10^{-95}	1.10×10^{-1}	8.17×10^{-22}	3.45×10^{-83}	3.40×10^{-39}	2.94×10^{-68}	1.10×10^1
10^7	2.00×10^9	4.06×10^{-2}	5.61×10^{-49}	1.42×10^{-1}	9.33×10^{-13}	3.53×10^{-42}	2.31×10^{-21}	1.81×10^{-35}	1.14×10^1
10^7	3.00×10^9	4.38×10^{-2}	2.80×10^{-33}	1.66×10^{-1}	1.59×10^{-9}	3.01×10^{-28}	3.85×10^{-15}	2.48×10^{-24}	1.22×10^1
10^7	5.00×10^9	6.12×10^{-2}	1.87×10^{-20}	2.87×10^{-1}	1.26×10^{-6}	1.04×10^{-16}	8.49×10^{-10}	7.24×10^{-15}	1.36×10^1
10^7	1.00×10^{10}	1.18×10^0	4.00×10^{-10}	6.43×10^0	3.29×10^{-3}	1.36×10^{-7}	1.05×10^{-4}	4.13×10^{-7}	2.75×10^1
10^7	1.50×10^{10}	9.02×10^0	2.89×10^{-6}	3.94×10^1	2.36×10^{-1}	2.29×10^{-4}	2.16×10^{-2}	2.14×10^{-4}	8.69×10^1
10^7	2.00×10^{10}	3.56×10^1	3.33×10^{-4}	1.40×10^2	3.14×10^0	1.15×10^{-2}	4.78×10^{-1}	6.11×10^{-3}	2.42×10^2
10^7	2.50×10^{10}	9.75×10^1	6.50×10^{-3}	3.74×10^2	1.82×10^1	1.33×10^{-1}	3.62×10^0	5.37×10^{-2}	5.69×10^2
10^7	3.00×10^{10}	2.14×10^2	5.06×10^{-2}	8.32×10^2	6.67×10^1	7.24×10^{-1}	1.53×10^1	2.56×10^{-1}	1.18×10^3
10^{11}	1.00×10^7	1.00×10^{100}	1.73×10^1	1.00×10^{-100}	4.70×10^5	1.00×10^{-100}	3.45×10^3	1.00×10^{-100}	3.11×10^9
10^{11}	4.00×10^8	1.00×10^{100}	1.73×10^1	1.00×10^{-100}	4.67×10^5	1.00×10^{-100}	3.44×10^3	1.00×10^{-100}	3.06×10^5
10^{11}	7.00×10^8	1.00×10^{100}	1.73×10^1	1.00×10^{-100}	4.66×10^5	1.00×10^{-100}	3.44×10^3	1.00×10^{-100}	3.09×10^5
10^{11}	1.00×10^9	1.00×10^{100}	1.73×10^1	1.00×10^{-100}	4.65×10^5	1.00×10^{-100}	3.44×10^3	1.00×10^{-100}	3.09×10^5
10^{11}	2.00×10^9	9.44×10^{-55}	1.77×10^1	2.47×10^{-58}	4.34×10^5	1.26×10^{-99}	3.44×10^3	6.46×10^{-93}	3.20×10^5
10^{11}	3.00×10^9	4.63×10^{-37}	1.82×10^1	2.30×10^{-39}	3.83×10^5	1.00×10^{-66}	3.46×10^3	8.24×10^{-63}	3.40×10^5
10^{11}	5.00×10^9	1.34×10^{-22}	1.99×10^1	4.29×10^{-24}	2.99×10^5	4.20×10^{-40}	3.49×10^3	2.91×10^{-38}	3.77×10^5
10^{11}	1.00×10^{10}	3.06×10^{-11}	2.85×10^1	9.16×10^{-12}	2.04×10^5	1.67×10^{-19}	3.75×10^3	5.06×10^{-19}	4.19×10^5
10^{11}	1.50×10^{10}	3.93×10^{-7}	4.88×10^1	4.79×10^{-7}	1.67×10^5	2.65×10^{-12}	5.30×10^3	2.48×10^{-12}	4.44×10^5
10^{11}	2.00×10^{10}	7.53×10^{-5}	8.73×10^1	1.76×10^{-4}	1.49×10^5	1.40×10^{-8}	9.12×10^3	7.41×10^{-9}	4.66×10^5
10^{11}	2.50×10^{10}	2.55×10^{-3}	1.42×10^2	7.85×10^{-3}	1.40×10^5				

Table 3 Calculated antineutrino and neutrino cooling rates due to weak rates on ^{20}O , ^{20}F , ^{20}Ne and ^{20}Na at different selected densities and temperatures in stellar environment. The first column shows the stellar densities (ρY_e) (in units of g.cm^{-3}). The rates are tabulated in units of MeV.s^{-1} .

ρY_e (g.cm^{-3})	T (K)	^{20}O		^{20}F		^{20}Ne		^{20}Na	
		$\lambda_{\bar{\nu}}$	λ_{ν}	$\lambda_{\bar{\nu}}$	λ_{ν}	$\lambda_{\bar{\nu}}$	λ_{ν}	$\lambda_{\bar{\nu}}$	λ_{ν}
10^1	1.00×10^7	7.94×10^{-2}	1.00×10^{-100}	5.41×10^{-2}	1.00×10^{-100}	1.00×10^{-100}	1.00×10^{-100}	1.00×10^{-100}	4.81×10^0
10^1	4.00×10^8	7.94×10^{-2}	1.00×10^{-100}	5.41×10^{-2}	7.74×10^{-60}	1.00×10^{-100}	1.00×10^{-100}	1.00×10^{-100}	4.81×10^0
10^1	7.00×10^8	7.94×10^{-2}	1.00×10^{-100}	5.40×10^{-2}	1.51×10^{-37}	1.00×10^{-100}	5.05×10^{-63}	1.52×10^{-83}	4.81×10^0
10^1	1.00×10^9	7.94×10^{-2}	1.37×10^{-98}	5.38×10^{-2}	2.04×10^{-27}	5.36×10^{-75}	2.72×10^{-45}	4.60×10^{-59}	4.82×10^0
10^1	2.00×10^9	8.04×10^{-2}	9.06×10^{-51}	5.50×10^{-2}	5.56×10^{-15}	3.58×10^{-38}	5.78×10^{-24}	2.32×10^{-30}	4.99×10^0
10^1	3.00×10^9	8.75×10^{-2}	2.00×10^{-34}	8.05×10^{-2}	1.68×10^{-10}	1.21×10^{-25}	1.86×10^{-16}	1.21×10^{-20}	5.33×10^0
10^1	5.00×10^9	1.77×10^{-1}	8.20×10^{-21}	3.74×10^{-1}	1.50×10^{-6}	2.74×10^{-15}	5.60×10^{-10}	1.16×10^{-12}	6.22×10^0
10^1	1.00×10^{10}	3.15×10^0	8.97×10^{-10}	7.06×10^0	7.80×10^{-3}	7.64×10^{-7}	2.95×10^{-4}	4.01×10^{-6}	2.19×10^1
10^1	1.50×10^{10}	2.74×10^1	1.11×10^{-5}	4.76×10^1	4.63×10^{-1}	1.33×10^{-3}	7.45×10^{-2}	1.60×10^{-3}	1.16×10^2
10^1	2.00×10^{10}	1.37×10^2	1.86×10^{-3}	1.97×10^2	6.50×10^0	8.45×10^{-2}	1.90×10^0	5.64×10^{-2}	4.24×10^2
10^1	2.50×10^{10}	4.85×10^2	4.95×10^{-2}	6.12×10^2	4.34×10^1	1.26×10^0	1.66×10^1	6.78×10^{-1}	1.24×10^3
10^1	3.00×10^{10}	1.37×10^3	5.06×10^{-1}	1.57×10^3	1.86×10^2	8.83×10^0	8.15×10^1	4.48×10^0	3.15×10^3
10^4	1.00×10^7	7.94×10^{-2}	1.00×10^{-100}	5.36×10^{-2}	1.00×10^{-100}	1.00×10^{-100}	1.00×10^{-100}	4.81×10^0	4.81×10^0
10^4	4.00×10^8	7.94×10^{-2}	1.00×10^{-100}	5.38×10^{-2}	8.02×10^{-57}	1.00×10^{-100}	1.00×10^{-100}	4.81×10^0	4.81×10^0
10^4	7.00×10^8	7.94×10^{-2}	1.00×10^{-100}	5.38×10^{-2}	3.52×10^{-35}	1.00×10^{-100}	1.17×10^{-60}	6.50×10^{-86}	4.81×10^0
10^4	1.00×10^9	7.94×10^{-2}	2.32×10^{-98}	5.37×10^{-2}	2.29×10^{-26}	4.78×10^{-76}	3.05×10^{-44}	4.10×10^{-60}	4.82×10^0
10^4	2.00×10^9	8.04×10^{-2}	9.14×10^{-51}	5.46×10^{-2}	6.03×10^{-15}	3.30×10^{-38}	6.27×10^{-24}	2.14×10^{-30}	4.99×10^0
10^4	3.00×10^9	8.75×10^{-2}	2.00×10^{-34}	8.00×10^{-2}	1.71×10^{-10}	1.19×10^{-25}	1.89×10^{-16}	1.19×10^{-20}	5.33×10^0
10^4	5.00×10^9	1.77×10^{-1}	8.22×10^{-21}	3.73×10^{-1}	1.50×10^{-6}	2.74×10^{-15}	5.62×10^{-10}	1.16×10^{-12}	6.22×10^0
10^4	1.00×10^{10}	3.16×10^0	9.02×10^{-10}	7.08×10^0	7.82×10^{-3}	7.67×10^{-7}	2.96×10^{-4}	4.02×10^{-6}	2.19×10^1
10^4	1.50×10^{10}	2.74×10^1	1.11×10^{-5}	4.79×10^1	4.66×10^{-1}	1.33×10^{-3}	7.46×10^{-2}	1.61×10^{-3}	1.16×10^2
10^4	2.00×10^{10}	1.37×10^2	1.87×10^{-3}	1.98×10^2	6.53×10^0	8.49×10^{-2}	1.91×10^0	5.66×10^{-2}	4.25×10^2
10^4	2.50×10^{10}	4.88×10^2	4.98×10^{-2}	6.14×10^2	4.36×10^1	1.27×10^0	1.67×10^1	6.81×10^{-1}	1.25×10^3
10^4	3.00×10^{10}	1.37×10^3	5.08×10^{-1}	1.58×10^3	1.87×10^2	8.87×10^0	8.18×10^1	4.50×10^0	3.16×10^3
10^7	1.00×10^7	5.18×10^{-2}	1.00×10^{-100}	6.17×10^{-3}	1.00×10^{-100}	1.00×10^{-100}	1.00×10^{-100}	6.11×10^0	6.11×10^0
10^7	4.00×10^8	5.18×10^{-2}	1.00×10^{-100}	6.62×10^{-3}	4.63×10^{-47}	1.00×10^{-100}	2.44×10^{-91}	1.00×10^{-100}	6.11×10^0
10^7	7.00×10^8	5.21×10^{-2}	1.00×10^{-100}	7.46×10^{-3}	7.03×10^{-29}	1.00×10^{-100}	2.00×10^{-54}	3.26×10^{-92}	6.12×10^0
10^7	1.00×10^9	5.27×10^{-2}	1.53×10^{-92}	8.69×10^{-3}	2.28×10^{-21}	4.80×10^{-81}	2.47×10^{-39}	4.13×10^{-65}	6.14×10^0
10^7	2.00×10^9	5.53×10^{-2}	6.52×10^{-48}	1.39×10^{-2}	4.00×10^{-12}	4.99×10^{-41}	3.64×10^{-21}	3.24×10^{-33}	6.40×10^0
10^7	3.00×10^9	5.89×10^{-2}	1.04×10^{-32}	1.88×10^{-2}	8.75×10^{-9}	2.32×10^{-27}	9.16×10^{-15}	2.32×10^{-22}	6.85×10^0
10^7	5.00×10^9	8.49×10^{-2}	4.16×10^{-20}	9.10×10^{-2}	7.59×10^{-6}	5.42×10^{-16}	2.80×10^{-9}	2.31×10^{-13}	7.87×10^0
10^7	1.00×10^{10}	2.55×10^0	1.13×10^{-9}	5.68×10^0	9.82×10^{-3}	6.11×10^{-7}	3.72×10^{-4}	3.20×10^{-6}	2.42×10^1
10^7	1.50×10^{10}	2.58×10^1	1.19×10^{-5}	4.49×10^1	4.97×10^{-1}	1.25×10^{-3}	7.98×10^{-2}	1.51×10^{-3}	1.21×10^2
10^7	2.00×10^{10}	1.34×10^2	1.92×10^{-3}	1.93×10^2	6.71×10^0	8.26×10^{-2}	1.96×10^0	5.51×10^{-2}	4.34×10^2
10^7	2.50×10^{10}	4.81×10^2	5.05×10^{-2}	6.07×10^2	4.42×10^1	1.25×10^0	1.69×10^1	6.71×10^{-1}	1.26×10^3
10^7	3.00×10^{10}	1.36×10^3	5.13×10^{-1}	1.57×10^3	1.88×10^2	8.81×10^0	8.26×10^1	4.47×10^0	3.18×10^3
10^{11}	1.00×10^7	1.00×10^{-100}	3.16×10^1	1.00×10^{-100}	1.02×10^6	1.00×10^{-100}	1.48×10^4	1.00×10^{-100}	1.11×10^6
10^{11}	4.00×10^8	1.00×10^{-100}	3.17×10^1	1.00×10^{-100}	1.01×10^6	1.00×10^{-100}	1.47×10^4	1.00×10^{-100}	1.10×10^6
10^{11}	7.00×10^8	1.00×10^{-100}	3.18×10^1	1.00×10^{-100}	1.01×10^6	1.00×10^{-100}	1.47×10^4	1.00×10^{-100}	1.11×10^6
10^{11}	1.00×10^9	1.00×10^{-100}	3.20×10^1	1.00×10^{-100}	1.00×10^6	1.00×10^{-100}	1.48×10^4	1.00×10^{-100}	1.11×10^6
10^{11}	2.00×10^9	6.31×10^{-54}	3.31×10^1	1.74×10^{-59}	9.42×10^5	1.78×10^{-98}	1.48×10^4	1.16×10^{-90}	1.16×10^6
10^{11}	3.00×10^9	1.22×10^{-36}	3.51×10^1	2.14×10^{-40}	8.34×10^5	7.73×10^{-66}	1.49×10^4	7.73×10^{-61}	1.26×10^6
10^{11}	5.00×10^9	2.47×10^{-22}	4.17×10^1	7.66×10^{-25}	6.64×10^5	2.18×10^{-39}	1.52×10^4	9.27×10^{-37}	1.42×10^6
10^{11}	1.00×10^{10}	5.90×10^{-11}	8.43×10^1	7.31×10^{-12}	4.94×10^5	7.48×10^{-19}	1.74×10^4	3.92×10^{-18}	1.64×10^6
10^{11}	1.50×10^{10}	8.85×10^{-7}	2.44×10^2	5.33×10^{-7}	4.56×10^5	1.45×10^{-11}	3.03×10^4	1.75×10^{-11}	1.87×10^6
10^{11}	2.00×10^{10}	2.30×10^{-4}	6.73×10^2	2.39×10^{-4}	4.59×10^5	1.00×10^{-7}	6.25×10^4	6.68×10^{-8}	2.11×10^6
10^{11}	2.50×10^{10}	1.11×10^{-2}	1.47×10^3	1.26×10^{-2}	4.84×10^5	2.56×10^{-5}	1.08×10^5	1.37×10^{-5}	2.36×10^6
10^{11}	3.00×10^{10}	1.97×10^{-1}	2.68×10^3	2.18×10^{-1}	5.26×10^5	1.21×10^{-3}	1.59×10^5	6.12×10^{-4}	2.60×10^6

Table 4 Same as Table. 2, but for ^{23}O , ^{23}F , ^{23}Ne , ^{23}Na and ^{23}Mg

ρY_e (g.cm $^{-3}$)	T (K)	^{23}O		^{23}F		^{23}Ne		^{23}Na		^{23}Mg	
		λ_{γ}^B	λ_{γ}^{EC}								
10^1	1.00×10^7	4.44×10^1	1.00×10^{-100}	1.58×10^0	1.00×10^{-100}	1.16×10^{-2}	1.00×10^{-100}	1.00×10^{-100}	1.00×10^{-100}	1.00×10^{-100}	4.79×10^{-2}
10^1	4.00×10^8	4.44×10^1	1.00×10^{-100}	1.58×10^0	1.00×10^{-100}	1.16×10^{-2}	1.00×10^{-100}	4.28×10^{-70}	6.68×10^{-67}	1.00×10^{-100}	4.19×10^{-2}
10^1	7.00×10^8	4.44×10^1	1.00×10^{-100}	1.58×10^0	3.07×10^{-91}	1.16×10^{-2}	8.02×10^{-71}	9.12×10^{-45}	3.52×10^{-42}	1.00×10^{-100}	3.61×10^{-2}
10^1	1.00×10^9	4.44×10^1	1.00×10^{-100}	1.58×10^0	1.01×10^{-64}	1.16×10^{-2}	8.34×10^{-51}	2.62×10^{-32}	3.73×10^{-31}	1.81×10^{-75}	3.29×10^{-2}
10^1	2.00×10^9	4.30×10^1	4.60×10^{-71}	1.58×10^0	2.47×10^{-33}	1.25×10^{-2}	8.65×10^{-27}	1.26×10^{-17}	9.33×10^{-18}	4.63×10^{-43}	3.02×10^{-2}
10^1	3.00×10^9	4.05×10^1	6.95×10^{-48}	1.60×10^0	1.28×10^{-22}	1.67×10^{-2}	2.20×10^{-18}	1.37×10^{-12}	1.13×10^{-12}	3.92×10^{-32}	3.76×10^{-2}
10^1	5.00×10^9	3.67×10^1	4.12×10^{-29}	1.79×10^0	9.57×10^{-14}	5.45×10^{-2}	3.08×10^{-11}	4.43×10^{-8}	4.92×10^{-8}	3.19×10^{-23}	1.25×10^{-1}
10^1	1.00×10^{10}	4.12×10^1	2.14×10^{-14}	5.41×10^0	1.65×10^{-6}	1.30×10^0	4.13×10^{-5}	8.09×10^{-4}	8.97×10^{-4}	3.47×10^{-16}	2.26×10^0
10^1	1.50×10^{10}	7.94×10^1	1.56×10^{-9}	1.95×10^1	9.14×10^{-4}	1.16×10^1	1.17×10^{-2}	5.46×10^{-2}	7.08×10^{-2}	1.28×10^{-13}	1.79×10^1
10^1	2.00×10^{10}	1.83×10^2	5.96×10^{-7}	5.20×10^1	2.96×10^{-2}	5.41×10^1	2.92×10^{-1}	7.03×10^{-1}	9.86×10^{-1}	3.18×10^{-12}	9.44×10^1
10^1	2.50×10^{10}	3.98×10^2	3.11×10^{-5}	1.11×10^2	2.82×10^{-1}	1.72×10^2	2.48×10^0	4.14×10^0	6.00×10^0	2.54×10^{-11}	3.56×10^2
10^1	3.00×10^{10}	7.82×10^2	4.02×10^{-4}	2.07×10^2	1.43×10^0	4.32×10^2	1.17×10^1	1.56×10^1	2.30×10^1	1.12×10^{-10}	1.03×10^3
10^4	1.00×10^7	4.44×10^1	1.00×10^{-100}	1.58×10^0	1.00×10^{-100}	1.15×10^{-2}	1.00×10^{-100}	1.00×10^{-100}	1.00×10^{-100}	1.00×10^{-100}	4.86×10^{-2}
10^4	4.00×10^8	4.44×10^1	1.00×10^{-100}	1.58×10^0	1.00×10^{-100}	1.15×10^{-2}	1.00×10^{-100}	4.92×10^{-72}	6.92×10^{-64}	1.00×10^{-100}	4.22×10^{-2}
10^4	7.00×10^8	4.44×10^1	1.00×10^{-100}	1.58×10^0	7.16×10^{-89}	1.15×10^{-2}	1.87×10^{-68}	3.94×10^{-47}	8.22×10^{-40}	1.00×10^{-100}	3.63×10^{-2}
10^4	1.00×10^9	4.44×10^1	1.00×10^{-100}	1.58×10^0	1.14×10^{-63}	1.16×10^{-2}	9.33×10^{-50}	2.33×10^{-33}	4.19×10^{-30}	1.61×10^{-76}	3.32×10^{-2}
10^4	2.00×10^9	4.30×10^1	4.73×10^{-71}	1.58×10^0	2.67×10^{-33}	1.24×10^{-2}	9.38×10^{-27}	1.17×10^{-17}	1.01×10^{-17}	4.28×10^{-43}	3.03×10^{-2}
10^4	3.00×10^9	4.05×10^1	7.14×10^{-48}	1.60×10^0	1.30×10^{-22}	1.66×10^{-2}	2.23×10^{-18}	1.35×10^{-12}	1.15×10^{-12}	3.86×10^{-32}	3.78×10^{-2}
10^4	5.00×10^9	3.67×10^1	4.21×10^{-29}	1.79×10^0	9.59×10^{-14}	5.43×10^{-2}	3.08×10^{-11}	4.43×10^{-8}	4.93×10^{-8}	3.19×10^{-23}	1.25×10^{-1}
10^4	1.00×10^{10}	4.12×10^1	2.24×10^{-14}	5.42×10^0	1.65×10^{-6}	1.30×10^0	4.13×10^{-5}	8.09×10^{-4}	8.97×10^{-4}	3.47×10^{-16}	2.26×10^0
10^4	1.50×10^{10}	7.94×10^1	1.62×10^{-9}	1.95×10^1	9.16×10^{-4}	1.16×10^1	1.17×10^{-2}	5.46×10^{-2}	7.08×10^{-2}	1.29×10^{-13}	1.80×10^1
10^4	2.00×10^{10}	1.84×10^2	6.05×10^{-7}	5.20×10^1	2.96×10^{-2}	5.41×10^1	2.92×10^{-1}	7.05×10^{-1}	9.86×10^{-1}	3.18×10^{-12}	9.44×10^1
10^4	2.50×10^{10}	3.98×10^2	3.13×10^{-5}	1.11×10^2	2.83×10^{-1}	1.73×10^2	2.48×10^0	4.14×10^0	6.01×10^0	2.54×10^{-11}	3.56×10^2
10^4	3.00×10^{10}	7.82×10^2	4.11×10^{-4}	2.08×10^2	1.43×10^0	4.32×10^2	1.18×10^1	1.56×10^1	2.30×10^1	1.12×10^{-10}	1.03×10^3
10^7	1.00×10^7	4.12×10^1	1.00×10^{-100}	1.18×10^0	1.00×10^{-100}	5.25×10^{-3}	1.00×10^{-100}	1.00×10^{-100}	1.00×10^{-100}	1.00×10^{-100}	4.33×10^{-1}
10^7	4.00×10^8	4.12×10^1	1.00×10^{-100}	1.18×10^0	1.00×10^{-100}	5.30×10^{-3}	1.00×10^{-100}	5.37×10^{-80}	4.00×10^{-54}	1.00×10^{-100}	3.90×10^{-1}
10^7	7.00×10^8	4.13×10^1	1.00×10^{-100}	1.19×10^0	1.43×10^{-82}	5.41×10^{-3}	3.73×10^{-62}	3.13×10^{-53}	1.64×10^{-33}	1.00×10^{-100}	3.52×10^{-1}
10^7	1.00×10^9	4.12×10^1	1.00×10^{-100}	1.19×10^0	1.13×10^{-58}	5.60×10^{-3}	9.29×10^{-45}	2.34×10^{-38}	4.17×10^{-25}	1.62×10^{-81}	3.34×10^{-1}
10^7	2.00×10^9	4.01×10^1	3.41×10^{-68}	1.22×10^0	1.77×10^{-30}	6.97×10^{-3}	6.21×10^{-24}	1.76×10^{-20}	6.70×10^{-15}	6.46×10^{-46}	3.28×10^{-1}
10^7	3.00×10^9	3.79×10^1	3.52×10^{-46}	1.26×10^0	6.67×10^{-21}	9.57×10^{-3}	1.14×10^{-16}	2.63×10^{-14}	5.89×10^{-11}	7.53×10^{-34}	3.54×10^{-1}
10^7	5.00×10^9	3.44×10^1	2.08×10^{-28}	1.39×10^0	4.84×10^{-13}	2.39×10^{-2}	1.56×10^{-10}	8.77×10^{-9}	2.48×10^{-7}	6.32×10^{-24}	4.76×10^{-1}
10^7	1.00×10^{10}	3.85×10^1	2.51×10^{-14}	4.57×10^0	2.07×10^{-6}	1.05×10^0	5.19×10^{-5}	6.46×10^{-4}	1.12×10^{-3}	2.76×10^{-16}	2.81×10^0
10^7	1.50×10^{10}	7.60×10^1	1.83×10^{-9}	1.84×10^1	9.77×10^{-4}	1.09×10^1	1.25×10^{-2}	5.11×10^{-2}	7.55×10^{-2}	1.20×10^{-13}	1.91×10^1
10^7	2.00×10^{10}	1.79×10^2	6.21×10^{-7}	5.07×10^1	3.05×10^{-2}	5.27×10^1	3.00×10^{-1}	6.85×10^{-1}	1.01×10^0	3.10×10^{-12}	9.71×10^1
10^7	2.50×10^{10}	3.94×10^2	3.23×10^{-5}	1.10×10^2	2.87×10^{-1}	1.70×10^2	2.52×10^0	4.08×10^0	6.10×10^0	2.51×10^{-11}	3.61×10^2
10^7	3.00×10^{10}	7.76×10^2	4.19×10^{-4}	2.07×10^2	4.29×10^0	1.19×10^1	1.55×10^1	2.32×10^1	1.11×10^{-10}	1.04×10^3	
10^{11}	1.00×10^7	1.00×10^{-100}	1.00×10^{-100}	1.00×10^{-100}	1.00×10^{-100}	7.08×10^3	1.00×10^{-100}	1.10×10^3	1.00×10^{-100}	3.27×10^9	
10^{11}	4.00×10^8	1.00×10^{-100}	4.92×10^{-44}	1.00×10^{-100}	8.63×10^{-21}	1.00×10^{-100}	7.06×10^3	1.00×10^{-100}	1.09×10^3	1.00×10^{-100}	3.15×10^5
10^{11}	7.00×10^8	1.00×10^{-100}	7.46×10^{-27}	1.00×10^{-100}	8.63×10^{-11}	1.00×10^{-100}	7.06×10^3	1.00×10^{-100}	1.11×10^3	1.00×10^{-100}	3.10×10^5
10^{11}	1.00×10^9	3.01×10^{-92}	7.34×10^{-20}	1.11×10^{-81}	8.65×10^{-7}	1.00×10^{-100}	7.06×10^3	1.00×10^{-100}	1.19×10^3	1.00×10^{-100}	3.06×10^5
10^{11}	2.00×10^9	3.88×10^{-47}	3.12×10^{-11}	2.98×10^{-42}	4.02×10^{-2}	7.74×10^{-53}	6.93×10^3	6.30×10^{-78}	1.91×10^3	1.00×10^{-100}	3.01×10^5
10^{11}	3.00×10^9	1.04×10^{-31}	3.53×10^{-8}	7.08×10^{-29}	1.46×10^0	5.78×10^{-36}	6.70×10^3	8.77×10^{-53}	2.65×10^3	2.51×10^{-72}	3.00×10^5
10^{11}	5.00×10^9	5.62×10^{-19}	1.74×10^{-5}	6.78×10^{-18}	2.70×10^1	$2.82 \times 10^{-$					

Table 5 Same as Table. 3, but for ^{23}O , ^{23}F , ^{23}Ne , ^{23}Na and ^{23}Mg

ρY_e (g.cm^{-3})	T (K)	^{23}O		^{23}F		^{23}Ne		^{23}Na		^{23}Mg	
		$\lambda_{\bar{p}}$	λ_{ν}	$\lambda_{\bar{p}}$	λ_{ν}	$\lambda_{\bar{p}}$	λ_{ν}	$\lambda_{\bar{p}}$	λ_{ν}	$\lambda_{\bar{p}}$	λ_{ν}
10^1	1.00×10^7	1.73×10^4	1.00×10^{-100}	4.28×10^{-1}	1.00×10^{-100}	4.05×10^{-2}	1.00×10^{-100}	1.00×10^{-100}	1.00×10^{-100}	1.00×10^{-100}	8.13×10^{-2}
10^1	4.00×10^8	1.73×10^4	1.00×10^{-100}	4.28×10^{-1}	1.00×10^{-100}	4.05×10^{-2}	1.00×10^{-100}	1.99×10^{-60}	6.58×10^{-66}	1.00×10^{-100}	7.26×10^{-2}
10^1	7.00×10^8	1.73×10^4	1.00×10^{-100}	4.28×10^{-1}	3.21×10^{-89}	4.05×10^{-2}	1.11×10^{-69}	6.50×10^{-36}	5.46×10^{-41}	3.98×10^{-93}	6.43×10^{-2}
10^1	1.00×10^9	1.73×10^4	1.00×10^{-100}	4.28×10^{-1}	4.19×10^{-63}	4.06×10^{-2}	1.13×10^{-49}	2.44×10^{-26}	8.02×10^{-30}	2.03×10^{-65}	5.97×10^{-2}
10^1	2.00×10^9	1.68×10^4	1.57×10^{-77}	4.31×10^{-1}	4.91×10^{-32}	4.27×10^{-2}	9.91×10^{-26}	1.67×10^{-14}	3.09×10^{-16}	5.83×10^{-33}	5.69×10^{-2}
10^1	3.00×10^9	1.60×10^4	6.07×10^{-52}	4.54×10^{-1}	2.49×10^{-21}	5.36×10^{-2}	2.09×10^{-17}	2.20×10^{-10}	2.19×10^{-11}	5.61×10^{-22}	7.41×10^{-2}
10^1	5.00×10^9	1.51×10^4	4.75×10^{-31}	7.50×10^{-1}	2.18×10^{-12}	1.28×10^{-1}	2.32×10^{-10}	7.85×10^{-7}	4.13×10^{-7}	6.10×10^{-13}	2.83×10^{-1}
10^1	1.00×10^{10}	2.83×10^4	1.27×10^{-14}	8.18×10^0	4.57×10^{-5}	1.74×10^0	2.33×10^{-4}	2.12×10^{-3}	4.21×10^{-3}	1.32×10^{-5}	6.62×10^0
10^1	1.50×10^{10}	1.06×10^2	1.04×10^{-8}	6.12×10^1	2.69×10^{-2}	1.72×10^1	6.40×10^{-2}	1.17×10^{-1}	3.05×10^{-1}	8.59×10^{-3}	5.65×10^1
10^1	2.00×10^{10}	3.66×10^2	1.55×10^{-5}	3.01×10^2	9.25×10^{-1}	1.02×10^2	1.71×10^0	1.79×10^0	4.65×10^0	3.54×10^{-1}	3.01×10^2
10^1	2.50×10^{10}	1.05×10^3	1.64×10^{-3}	1.10×10^3	9.55×10^0	4.21×10^2	1.59×10^1	1.43×10^1	3.29×10^1	4.55×10^0	1.19×10^3
10^1	3.00×10^{10}	2.57×10^3	4.45×10^{-2}	3.25×10^3	5.25×10^1	1.35×10^3	8.39×10^1	7.48×10^1	1.48×10^2	3.12×10^1	3.78×10^3
10^4	1.00×10^7	1.73×10^4	1.00×10^{-100}	4.28×10^{-1}	1.00×10^{-100}	4.05×10^{-2}	1.00×10^{-100}	1.00×10^{-63}	1.00×10^{-100}	1.00×10^{-100}	8.30×10^{-2}
10^4	4.00×10^8	1.73×10^4	1.00×10^{-100}	4.28×10^{-1}	1.00×10^{-100}	4.05×10^{-2}	1.00×10^{-100}	3.71×10^{-63}	6.81×10^{-63}	1.00×10^{-100}	7.35×10^{-2}
10^4	7.00×10^8	1.73×10^4	1.00×10^{-100}	4.28×10^{-1}	7.48×10^{-87}	4.05×10^{-2}	2.59×10^{-67}	2.82×10^{-38}	1.27×10^{-38}	1.71×10^{-95}	6.49×10^{-2}
10^4	1.00×10^9	1.73×10^4	1.00×10^{-100}	4.28×10^{-1}	4.71×10^{-62}	4.05×10^{-2}	1.27×10^{-48}	2.18×10^{-27}	8.99×10^{-29}	1.81×10^{-66}	6.03×10^{-2}
10^4	2.00×10^9	1.68×10^4	1.70×10^{-77}	4.31×10^{-1}	5.32×10^{-32}	4.26×10^{-2}	1.08×10^{-25}	1.54×10^{-14}	3.35×10^{-16}	5.38×10^{-33}	5.71×10^{-2}
10^4	3.00×10^9	1.60×10^4	6.17×10^{-52}	4.53×10^{-1}	2.53×10^{-21}	5.36×10^{-2}	2.12×10^{-17}	2.18×10^{-10}	2.22×10^{-11}	5.53×10^{-22}	7.45×10^{-2}
10^4	5.00×10^9	1.51×10^4	4.78×10^{-31}	7.48×10^{-1}	2.19×10^{-12}	1.28×10^{-1}	2.32×10^{-10}	7.85×10^{-7}	4.15×10^{-7}	6.08×10^{-13}	2.84×10^{-1}
10^4	1.00×10^{10}	2.83×10^4	1.28×10^{-14}	8.20×10^0	4.58×10^{-5}	1.75×10^0	2.34×10^{-4}	2.13×10^{-3}	4.23×10^{-3}	1.32×10^{-5}	6.64×10^0
10^4	1.50×10^{10}	1.06×10^2	1.05×10^{-8}	6.14×10^1	2.69×10^{-2}	1.73×10^1	6.43×10^{-2}	1.17×10^{-1}	3.05×10^{-1}	8.61×10^{-3}	5.68×10^1
10^4	2.00×10^{10}	3.68×10^2	1.55×10^{-5}	3.02×10^2	9.27×10^{-1}	1.02×10^2	1.71×10^0	1.80×10^0	4.67×10^0	3.56×10^{-1}	3.02×10^2
10^4	2.50×10^{10}	1.05×10^3	1.65×10^{-3}	1.11×10^3	9.59×10^0	4.23×10^2	1.60×10^1	1.44×10^1	3.30×10^1	4.57×10^0	1.20×10^3
10^4	3.00×10^{10}	2.58×10^3	4.47×10^{-2}	3.27×10^3	5.27×10^1	1.36×10^3	8.43×10^1	7.52×10^1	1.48×10^2	3.13×10^1	3.80×10^3
10^7	1.00×10^7	1.53×10^4	1.00×10^{-100}	2.65×10^{-1}	1.00×10^{-100}	3.30×10^{-2}	1.00×10^{-100}	1.00×10^{-100}	1.00×10^{-100}	1.00×10^{-100}	9.71×10^{-1}
10^7	4.00×10^8	1.53×10^4	1.00×10^{-100}	2.67×10^{-1}	1.00×10^{-100}	3.30×10^{-2}	1.00×10^{-100}	4.73×10^{-71}	3.93×10^{-53}	1.00×10^{-100}	8.61×10^{-1}
10^7	7.00×10^8	1.53×10^4	1.00×10^{-100}	2.69×10^{-1}	1.50×10^{-80}	3.30×10^{-2}	5.16×10^{-61}	2.83×10^{-44}	2.54×10^{-32}	1.00×10^{-100}	7.66×10^{-1}
10^7	1.00×10^9	1.53×10^4	1.00×10^{-100}	2.72×10^{-1}	4.68×10^{-57}	3.32×10^{-2}	1.26×10^{-43}	2.26×10^{-32}	8.93×10^{-24}	1.82×10^{-71}	7.21×10^{-1}
10^7	2.00×10^9	1.50×10^4	1.12×10^{-74}	2.88×10^{-1}	3.52×10^{-29}	3.54×10^{-2}	7.13×10^{-23}	2.33×10^{-17}	2.22×10^{-13}	8.13×10^{-36}	7.08×10^{-1}
10^7	3.00×10^9	1.43×10^4	3.16×10^{-50}	3.10×10^{-1}	1.30×10^{-19}	4.45×10^{-2}	1.09×10^{-15}	4.25×10^{-12}	1.14×10^{-9}	1.08×10^{-23}	7.78×10^{-1}
10^7	5.00×10^9	1.34×10^4	2.41×10^{-30}	4.56×10^{-1}	1.10×10^{-11}	9.48×10^{-2}	1.17×10^{-9}	1.56×10^{-7}	2.09×10^{-6}	1.21×10^{-13}	1.13×10^0
10^7	1.00×10^{10}	2.48×10^4	1.60×10^{-14}	6.82×10^0	5.75×10^{-5}	1.45×10^0	2.93×10^{-4}	1.70×10^{-3}	5.30×10^{-3}	1.05×10^{-5}	8.26×10^0
10^7	1.50×10^{10}	1.00×10^2	1.12×10^{-8}	5.78×10^1	2.88×10^{-2}	1.63×10^1	6.87×10^{-2}	1.10×10^{-1}	3.27×10^{-1}	8.07×10^{-3}	6.04×10^1
10^7	2.00×10^{10}	3.59×10^2	1.60×10^{-5}	2.94×10^2	9.53×10^{-1}	1.76×10^0	1.75×10^0	4.80×10^0	3.46×10^0	3.10×10^2	
10^7	2.50×10^{10}	1.04×10^3	1.67×10^{-3}	1.09×10^3	9.73×10^0	4.17×10^2	1.62×10^1	1.42×10^1	3.34×10^1	4.51×10^0	1.21×10^3
10^7	3.00×10^{10}	2.56×10^3	4.51×10^{-2}	3.24×10^3	5.32×10^1	1.35×10^3	8.49×10^1	7.46×10^1	1.50×10^2	3.11×10^1	3.83×10^3
10^{11}	1.00×10^7	1.00×10^{-100}	1.00×10^{-100}	9.12×10^1	1.00×10^{-100}	2.49×10^4	1.00×10^{-100}	1.61×10^4	1.00×10^{-100}	1.00×10^{-100}	3.10×10^6
10^{11}	4.00×10^8	1.00×10^{-100}	6.58×10^{-77}	9.12×10^1	1.00×10^{-100}	2.48×10^4	1.00×10^{-100}	1.61×10^4	1.00×10^{-100}	1.00×10^{-100}	2.82×10^6
10^{11}	7.00×10^8	1.00×10^{-100}	1.82×10^{-45}	9.12×10^1	1.00×10^{-100}	2.48×10^4	1.00×10^{-100}	1.63×10^4	1.00×10^{-100}	1.00×10^{-100}	2.63×10^6
10^{11}	1.00×10^9	1.41×10^{-93}	1.17×10^{-32}	9.14×10^1	1.00×10^{-100}	2.48×10^4	1.00×10^{-100}	1.72×10^4	1.00×10^{-100}	1.00×10^{-100}	2.51×10^6
10^{11}	2.00×10^9	3.44×10^{-48}	3.11×10^{-17}	2.22×10^{-41}	9.29×10^1	5.43×10^{-52}	2.43×10^4	8.34×10^{-75}	2.61×10^4	2.90×10^{-93}	2.36×10^6
10^{11}	3.00×10^9	1.31×10^{-32}	9.10×10^{-12}	4.71×10^{-28}	1.04×10^2	2.90×10^{-35}	2.33×10^4	1.41×10^{-50}	3.61×10^4	3.60×10^{-62}	2.31×10^6
10^{11}	5.00×10^9	1.07×10^{-19}	5.48×10^{-7}	4.65×10^{-17}	2.89×10^2	1.38×10^{-21}	2.19×10^4	6.25×1			

Table 6 Same as Table. 2, but for ^{24}Ne , ^{24}Na and ^{24}Mg .

ρY_e (g.cm $^{-3}$)	T (K)	^{24}Ne		^{24}Na		^{24}Mg	
		λ_{γ}^{β}	λ_{γ}^{EC}	λ_{γ}^{β}	λ_{γ}^{EC}	λ_{γ}^{β}	λ_{γ}^{EC}
10^1	1.00×10^7	2.31×10^{-3}	1.00×10^{-100}	6.78×10^{-5}	1.00×10^{-100}	1.00×10^{-100}	1.00×10^{-100}
10^1	4.00×10^8	2.31×10^{-3}	1.00×10^{-100}	6.78×10^{-5}	9.86×10^{-52}	1.00×10^{-100}	1.32×10^{-83}
10^1	7.00×10^8	2.31×10^{-3}	1.00×10^{-100}	6.89×10^{-5}	1.08×10^{-32}	1.00×10^{-100}	1.47×10^{-51}
10^1	1.00×10^9	2.31×10^{-3}	8.36×10^{-77}	7.52×10^{-5}	6.28×10^{-24}	3.19×10^{-76}	1.44×10^{-37}
10^1	2.00×10^9	2.36×10^{-3}	5.15×10^{-40}	2.84×10^{-4}	3.59×10^{-13}	5.78×10^{-39}	1.08×10^{-20}
10^1	3.00×10^9	2.81×10^{-3}	2.07×10^{-27}	1.82×10^{-3}	2.88×10^{-9}	2.16×10^{-26}	1.21×10^{-14}
10^1	5.00×10^9	8.73×10^{-3}	6.24×10^{-17}	2.52×10^{-2}	8.53×10^{-6}	5.37×10^{-16}	3.40×10^{-9}
10^1	1.00×10^{10}	2.52×10^{-1}	2.40×10^{-8}	9.93×10^{-1}	1.58×10^{-2}	1.89×10^{-7}	3.64×10^{-4}
10^1	1.50×10^{10}	2.66×10^0	4.45×10^{-5}	8.93×10^0	5.81×10^{-1}	2.79×10^{-4}	5.90×10^{-2}
10^1	2.00×10^{10}	1.42×10^1	2.62×10^{-3}	4.19×10^1	5.85×10^0	1.37×10^{-2}	1.21×10^0
10^1	2.50×10^{10}	4.82×10^1	3.41×10^{-2}	1.36×10^2	3.01×10^1	1.57×10^{-1}	8.83×10^0
10^1	3.00×10^{10}	1.24×10^2	2.04×10^{-1}	3.46×10^2	1.04×10^2	8.61×10^{-1}	3.68×10^1
10^4	1.00×10^7	2.30×10^{-3}	1.00×10^{-100}	6.58×10^{-5}	1.00×10^{-100}	1.00×10^{-100}	1.00×10^{-100}
10^4	4.00×10^8	2.30×10^{-3}	1.00×10^{-100}	6.68×10^{-5}	1.02×10^{-48}	1.00×10^{-100}	1.37×10^{-80}
10^4	7.00×10^8	2.31×10^{-3}	1.00×10^{-100}	6.81×10^{-5}	2.51×10^{-30}	1.00×10^{-100}	3.43×10^{-49}
10^4	1.00×10^9	2.31×10^{-3}	9.38×10^{-76}	7.38×10^{-5}	7.05×10^{-23}	2.84×10^{-77}	1.61×10^{-36}
10^4	2.00×10^9	2.36×10^{-3}	5.58×10^{-40}	2.74×10^{-4}	3.89×10^{-13}	5.33×10^{-39}	1.17×10^{-20}
10^4	3.00×10^9	2.80×10^{-3}	2.09×10^{-27}	1.80×10^{-3}	2.92×10^{-9}	2.13×10^{-26}	1.23×10^{-14}
10^4	5.00×10^9	8.71×10^{-3}	6.27×10^{-17}	2.52×10^{-2}	8.55×10^{-6}	5.36×10^{-16}	3.41×10^{-9}
10^4	1.00×10^{10}	2.52×10^{-1}	2.40×10^{-8}	9.93×10^{-1}	1.58×10^{-2}	1.89×10^{-7}	3.64×10^{-4}
10^4	1.50×10^{10}	2.67×10^0	4.45×10^{-5}	8.93×10^0	5.82×10^{-1}	2.79×10^{-4}	5.90×10^{-2}
10^4	2.00×10^{10}	1.42×10^1	2.62×10^{-3}	4.20×10^1	5.86×10^0	1.37×10^{-2}	1.21×10^0
10^4	2.50×10^{10}	4.82×10^1	3.42×10^{-2}	1.36×10^2	3.01×10^1	1.58×10^{-1}	8.83×10^0
10^4	3.00×10^{10}	1.24×10^2	2.04×10^{-1}	3.46×10^2	1.04×10^2	8.61×10^{-1}	3.69×10^1
10^7	1.00×10^7	1.17×10^{-3}	1.00×10^{-100}	2.96×10^{-60}	1.00×10^{-100}	1.00×10^{-100}	1.00×10^{-100}
10^7	4.00×10^8	1.18×10^{-3}	1.00×10^{-100}	8.36×10^{-9}	5.89×10^{-39}	1.00×10^{-100}	2.39×10^{-71}
10^7	7.00×10^8	1.19×10^{-3}	3.50×10^{-99}	1.48×10^{-7}	5.02×10^{-24}	1.00×10^{-100}	3.87×10^{-43}
10^7	1.00×10^9	1.22×10^{-3}	9.33×10^{-71}	8.67×10^{-7}	7.01×10^{-18}	2.86×10^{-82}	1.16×10^{-31}
10^7	2.00×10^9	1.34×10^{-3}	3.70×10^{-37}	2.61×10^{-5}	2.58×10^{-10}	8.05×10^{-42}	7.01×10^{-18}
10^7	3.00×10^9	1.49×10^{-3}	1.07×10^{-25}	1.77×10^{-4}	1.50×10^{-7}	4.16×10^{-28}	6.01×10^{-13}
10^7	5.00×10^9	3.07×10^{-3}	3.16×10^{-16}	5.94×10^{-3}	4.32×10^{-5}	1.06×10^{-16}	1.70×10^{-8}
10^7	1.00×10^{10}	2.04×10^{-1}	3.02×10^{-8}	8.02×10^{-1}	1.99×10^{-2}	1.50×10^{-7}	4.56×10^{-4}
10^7	1.50×10^{10}	2.51×10^0	4.75×10^{-5}	8.39×10^0	6.21×10^{-1}	2.61×10^{-4}	6.30×10^{-2}
10^7	2.00×10^{10}	1.38×10^1	2.69×10^{-3}	4.08×10^1	6.03×10^0	1.33×10^{-2}	1.24×10^0
10^7	2.50×10^{10}	4.76×10^1	3.47×10^{-2}	1.34×10^2	3.05×10^1	1.56×10^{-1}	8.97×10^0
10^7	3.00×10^{10}	1.23×10^2	2.06×10^{-1}	3.44×10^2	1.05×10^2	8.55×10^{-1}	3.72×10^1
10^{11}	1.00×10^7	1.00×10^{-100}	9.18×10^1	1.00×10^{-100}	2.14×10^4	1.00×10^{-100}	1.00×10^4
10^{11}	4.00×10^8	1.00×10^{-100}	9.16×10^1	1.00×10^{-100}	2.13×10^4	1.00×10^{-100}	1.00×10^4
10^{11}	7.00×10^8	1.00×10^{-100}	9.16×10^1	1.00×10^{-100}	2.14×10^4	1.00×10^{-100}	1.00×10^4
10^{11}	1.00×10^9	1.00×10^{-100}	9.16×10^1	1.00×10^{-100}	2.21×10^4	1.00×10^{-100}	1.00×10^4
10^{11}	2.00×10^9	1.25×10^{-57}	9.23×10^1	1.06×10^{-60}	2.74×10^4	2.88×10^{-99}	1.01×10^4
10^{11}	3.00×10^9	3.22×10^{-39}	9.33×10^1	6.31×10^{-41}	3.33×10^4	1.39×10^{-66}	1.01×10^4
10^{11}	5.00×10^9	3.80×10^{-24}	9.68×10^1	6.97×10^{-25}	4.27×10^4	4.27×10^{-40}	1.02×10^4
10^{11}	1.00×10^{10}	2.67×10^{-12}	1.16×10^2	2.33×10^{-12}	6.43×10^4	1.84×10^{-19}	1.10×10^4
10^{11}	1.50×10^{10}	6.34×10^{-8}	1.76×10^2	1.19×10^{-7}	8.57×10^4	3.03×10^{-12}	1.49×10^4
10^{11}	2.00×10^{10}	2.14×10^{-5}	2.89×10^2	5.31×10^{-5}	1.04×10^5	1.62×10^{-8}	2.38×10^4
10^{11}	2.50×10^{10}	1.07×10^{-3}	4.28×10^2	2.84×10^{-3}	1.21×10^5	3.18×10^{-6}	3.51×10^4
10^{11}	3.00×10^{10}	1.79×10^{-2}	5.70×10^2	4.86×10^{-2}	1.35×10^5	1.17×10^{-4}	4.62×10^4

Table 7 Same as Table. 3, but for ^{24}Ne , ^{24}Na and ^{24}Mg .

ρY_e (g.cm $^{-3}$)	T (K)	^{24}Ne		^{24}Na		^{24}Mg	
		$\lambda_{\bar{\nu}}$	λ_{ν}	$\lambda_{\bar{\nu}}$	λ_{ν}	$\lambda_{\bar{\nu}}$	λ_{ν}
10 ¹	1.00×10^7	3.68×10^{-3}	1.00×10^{-100}	4.69×10^{-6}	1.00×10^{-100}	1.00×10^{-100}	1.00×10^{-100}
10 ¹	4.00×10^8	3.68×10^{-3}	1.00×10^{-100}	4.69×10^{-6}	1.18×10^{-52}	1.00×10^{-100}	6.67×10^{-84}
10 ¹	7.00×10^8	3.68×10^{-3}	1.00×10^{-100}	4.78×10^{-6}	2.29×10^{-33}	1.00×10^{-100}	1.28×10^{-51}
10 ¹	1.00×10^9	3.68×10^{-3}	8.28×10^{-76}	5.46×10^{-6}	1.90×10^{-24}	6.21×10^{-75}	1.83×10^{-37}
10 ¹	2.00×10^9	3.78×10^{-3}	4.02×10^{-39}	5.11×10^{-5}	2.06×10^{-13}	5.56×10^{-38}	2.94×10^{-20}
10 ¹	3.00×10^9	4.67×10^{-3}	1.57×10^{-26}	5.22×10^{-4}	2.33×10^{-9}	1.88×10^{-25}	4.43×10^{-14}
10 ¹	5.00×10^9	1.71×10^{-2}	4.65×10^{-16}	1.07×10^{-2}	1.05×10^{-5}	3.80×10^{-15}	1.29×10^{-8}
10 ¹	1.00×10^{10}	5.98×10^{-1}	1.67×10^{-7}	7.05×10^{-1}	3.03×10^{-2}	9.20×10^{-7}	1.30×10^{-3}
10 ¹	1.50×10^{10}	7.26×10^0	3.06×10^{-4}	8.67×10^0	1.21×10^0	1.57×10^{-3}	1.94×10^{-1}
10 ¹	2.00×10^{10}	4.86×10^1	2.00×10^{-2}	5.25×10^1	1.31×10^1	1.04×10^{-1}	3.94×10^0
10 ¹	2.50×10^{10}	2.17×10^2	3.06×10^{-1}	2.12×10^2	7.48×10^1	1.64×10^0	3.08×10^1
10 ¹	3.00×10^{10}	7.23×10^2	2.18×10^0	6.61×10^2	2.92×10^2	1.20×10^1	1.41×10^2
10 ⁴	1.00×10^7	3.66×10^{-3}	1.00×10^{-100}	4.51×10^{-6}	1.00×10^{-100}	1.00×10^{-100}	1.00×10^{-100}
10 ⁴	4.00×10^8	3.67×10^{-3}	1.00×10^{-100}	4.61×10^{-6}	1.22×10^{-49}	1.00×10^{-100}	6.89×10^{-81}
10 ⁴	7.00×10^8	3.67×10^{-3}	1.00×10^{-100}	4.71×10^{-6}	5.33×10^{-31}	1.00×10^{-100}	2.99×10^{-49}
10 ⁴	1.00×10^9	3.67×10^{-3}	9.29×10^{-75}	5.21×10^{-6}	2.13×10^{-23}	5.53×10^{-76}	2.06×10^{-36}
10 ⁴	2.00×10^9	3.78×10^{-3}	4.36×10^{-39}	4.82×10^{-5}	2.23×10^{-13}	5.13×10^{-38}	3.19×10^{-20}
10 ⁴	3.00×10^9	4.66×10^{-3}	1.59×10^{-26}	5.16×10^{-4}	2.37×10^{-9}	1.86×10^{-25}	4.50×10^{-14}
10 ⁴	5.00×10^9	1.71×10^{-2}	4.67×10^{-16}	1.07×10^{-2}	1.06×10^{-5}	3.80×10^{-15}	1.29×10^{-8}
10 ⁴	1.00×10^{10}	6.00×10^{-1}	1.67×10^{-7}	7.05×10^{-1}	3.04×10^{-2}	9.23×10^{-7}	1.30×10^{-3}
10 ⁴	1.50×10^{10}	7.28×10^0	3.07×10^{-4}	8.69×10^0	1.21×10^0	1.58×10^{-3}	1.95×10^{-1}
10 ⁴	2.00×10^{10}	4.89×10^1	2.00×10^{-2}	5.26×10^1	1.31×10^1	1.04×10^{-1}	3.94×10^0
10 ⁴	2.50×10^{10}	2.18×10^2	3.08×10^{-1}	2.13×10^2	7.52×10^1	1.64×10^0	3.08×10^1
10 ⁴	3.00×10^{10}	7.26×10^2	2.19×10^0	6.64×10^2	2.94×10^2	1.21×10^1	1.42×10^2
10 ⁷	1.00×10^7	1.36×10^{-3}	1.00×10^{-100}	1.56×10^{-63}	1.00×10^{-100}	1.00×10^{-100}	1.00×10^{-100}
10 ⁷	4.00×10^8	1.38×10^{-3}	1.00×10^{-100}	1.64×10^{-10}	7.06×10^{-40}	1.00×10^{-100}	1.83×10^{-71}
10 ⁷	7.00×10^8	1.42×10^{-3}	4.78×10^{-98}	5.08×10^{-9}	1.06×10^{-24}	1.00×10^{-100}	4.24×10^{-43}
10 ⁷	1.00×10^9	1.48×10^{-3}	9.25×10^{-70}	4.38×10^{-8}	2.12×10^{-18}	5.57×10^{-81}	1.71×10^{-31}
10 ⁷	2.00×10^9	1.75×10^{-3}	2.89×10^{-36}	2.42×10^{-6}	1.48×10^{-10}	7.74×10^{-41}	1.96×10^{-17}
10 ⁷	3.00×10^9	2.09×10^{-3}	8.15×10^{-25}	2.75×10^{-5}	1.22×10^{-7}	3.63×10^{-27}	2.18×10^{-12}
10 ⁷	5.00×10^9	5.41×10^{-3}	2.36×10^{-15}	2.33×10^{-3}	5.33×10^{-5}	7.53×10^{-16}	6.40×10^{-8}
10 ⁷	1.00×10^{10}	4.90×10^{-1}	2.10×10^{-7}	5.66×10^{-1}	3.81×10^{-2}	7.35×10^{-7}	1.63×10^{-3}
10 ⁷	1.50×10^{10}	6.85×10^0	3.28×10^{-4}	8.15×10^0	1.29×10^0	1.48×10^{-3}	2.08×10^{-1}
10 ⁷	2.00×10^{10}	4.75×10^1	2.06×10^{-2}	5.12×10^1	1.35×10^1	1.01×10^{-1}	4.06×10^0
10 ⁷	2.50×10^{10}	2.15×10^2	3.12×10^{-1}	2.10×10^2	7.62×10^1	1.62×10^0	3.13×10^1
10 ⁷	3.00×10^{10}	7.21×10^2	2.21×10^0	6.59×10^2	2.96×10^2	1.20×10^1	1.43×10^2
10 ¹¹	1.00×10^7	1.00×10^{-100}	1.27×10^2	1.00×10^{-100}	1.58×10^5	1.00×10^{-100}	3.78×10^4
10 ¹¹	4.00×10^8	1.00×10^{-100}	1.27×10^2	1.00×10^{-100}	1.58×10^5	1.00×10^{-100}	3.76×10^4
10 ¹¹	7.00×10^8	1.00×10^{-100}	1.27×10^2	1.00×10^{-100}	1.58×10^5	1.00×10^{-100}	3.76×10^4
10 ¹¹	1.00×10^9	1.00×10^{-100}	1.27×10^2	1.00×10^{-100}	1.61×10^5	1.00×10^{-100}	3.76×10^4
10 ¹¹	2.00×10^9	2.48×10^{-56}	1.29×10^2	9.95×10^{-62}	1.85×10^5	2.77×10^{-98}	3.78×10^4
10 ¹¹	3.00×10^9	5.05×10^{-38}	1.32×10^2	8.39×10^{-42}	2.10×10^5	1.21×10^{-65}	3.79×10^4
10 ¹¹	5.00×10^9	4.55×10^{-23}	1.41×10^2	1.42×10^{-25}	2.49×10^5	3.03×10^{-39}	3.85×10^4
10 ¹¹	1.00×10^{10}	2.18×10^{-11}	2.40×10^2	1.08×10^{-12}	3.25×10^5	8.99×10^{-19}	4.31×10^4
10 ¹¹	1.50×10^{10}	3.21×10^{-7}	8.79×10^2	1.02×10^{-7}	3.93×10^5	1.71×10^{-11}	6.61×10^4
10 ¹¹	2.00×10^{10}	8.45×10^{-5}	2.49×10^3	6.38×10^{-5}	4.59×10^5	1.23×10^{-7}	1.17×10^5
10 ¹¹	2.50×10^{10}	4.86×10^{-3}	4.90×10^3	4.37×10^{-3}	5.30×10^5	3.31×10^{-5}	1.86×10^5
10 ¹¹	3.00×10^{10}	1.03×10^{-1}	7.89×10^3	9.18×10^{-2}	6.10×10^5	1.64×10^{-3}	2.60×10^5

Table 8 Calculated γ -ray heating and antineutrino (neutrino) cooling rates due to weak rates on ^{25}Na and ^{25}Mg at different selected densities and temperatures in stellar environment. The first column shows the stellar densities (ρY_e) (in units of g.cm^{-3}). The rates are tabulated in units of MeV.s^{-1} .

ρY_e (g.cm^{-3})	T (K)	^{25}Na				^{25}Mg			
		λ_γ^β	λ_γ^{EC}	$\lambda_{\bar{\nu}}$	λ_ν	λ_γ^β	λ_γ^{EC}	$\lambda_{\bar{\nu}}$	λ_ν
10^1	1.00×10^7	1.51×10^{-2}	1.00×10^{-100}	3.46×10^{-2}	1.00×10^{-100}				
10^1	4.00×10^8	1.51×10^{-2}	1.00×10^{-100}	3.46×10^{-2}	1.00×10^{-100}	2.21×10^{-73}	5.35×10^{-68}	5.31×10^{-64}	5.62×10^{-59}
10^1	7.00×10^8	1.51×10^{-2}	4.72×10^{-62}	3.47×10^{-2}	2.43×10^{-64}	6.00×10^{-44}	1.44×10^{-43}	2.90×10^{-38}	4.85×10^{-37}
10^1	1.00×10^9	1.52×10^{-2}	1.33×10^{-44}	3.52×10^{-2}	2.52×10^{-46}	4.04×10^{-32}	1.71×10^{-31}	9.59×10^{-28}	4.59×10^{-27}
10^1	2.00×10^9	1.59×10^{-2}	1.17×10^{-23}	4.26×10^{-2}	7.82×10^{-25}	3.05×10^{-17}	6.65×10^{-17}	3.29×10^{-15}	7.85×10^{-15}
10^1	3.00×10^9	1.70×10^{-2}	2.45×10^{-16}	5.36×10^{-2}	2.84×10^{-17}	5.26×10^{-12}	9.29×10^{-12}	9.42×10^{-11}	2.18×10^{-10}
10^1	5.00×10^9	2.01×10^{-2}	5.16×10^{-10}	8.09×10^{-2}	1.88×10^{-10}	1.26×10^{-7}	2.53×10^{-7}	9.40×10^{-7}	2.09×10^{-6}
10^1	1.00×10^{10}	1.05×10^{-1}	3.51×10^{-4}	4.46×10^{-1}	1.92×10^{-4}	6.03×10^{-4}	2.70×10^{-3}	5.38×10^{-3}	1.16×10^{-2}
10^1	1.50×10^{10}	1.14×10^0	1.05×10^{-1}	3.37×10^0	4.43×10^{-2}	1.99×10^{-2}	1.87×10^{-1}	2.86×10^{-1}	5.93×10^{-1}
10^1	2.00×10^{10}	6.76×10^0	2.90×10^0	2.11×10^1	9.40×10^{-1}	1.63×10^{-1}	2.51×10^0	3.68×10^0	7.28×10^0
10^1	2.50×10^{10}	2.55×10^1	2.74×10^1	1.01×10^2	7.01×10^0	7.06×10^{-1}	1.51×10^1	2.37×10^1	4.50×10^1
10^1	3.00×10^{10}	7.19×10^1	1.44×10^2	3.81×10^2	3.00×10^1	2.15×10^0	5.75×10^1	1.01×10^2	1.86×10^2
10^4	1.00×10^7	1.51×10^{-2}	1.00×10^{-100}	3.46×10^{-2}	1.00×10^{-100}				
10^4	4.00×10^8	1.51×10^{-2}	1.15×10^{-99}	3.46×10^{-2}	1.00×10^{-100}	2.10×10^{-73}	5.53×10^{-65}	5.15×10^{-64}	5.82×10^{-56}
10^4	7.00×10^8	1.51×10^{-2}	1.10×10^{-59}	3.47×10^{-2}	5.68×10^{-62}	2.60×10^{-46}	3.37×10^{-41}	6.38×10^{-39}	1.13×10^{-34}
10^4	1.00×10^9	1.52×10^{-2}	1.50×10^{-43}	3.52×10^{-2}	2.82×10^{-45}	3.60×10^{-33}	1.92×10^{-30}	1.48×10^{-28}	5.15×10^{-26}
10^4	2.00×10^9	1.59×10^{-2}	1.27×10^{-23}	4.26×10^{-2}	8.49×10^{-25}	2.82×10^{-17}	7.21×10^{-17}	3.03×10^{-15}	8.53×10^{-15}
10^4	3.00×10^9	1.70×10^{-2}	2.48×10^{-16}	5.36×10^{-2}	2.88×10^{-17}	5.19×10^{-12}	9.42×10^{-12}	9.31×10^{-11}	2.21×10^{-10}
10^4	5.00×10^9	2.01×10^{-2}	5.19×10^{-10}	8.09×10^{-2}	1.89×10^{-10}	1.26×10^{-7}	2.54×10^{-7}	9.40×10^{-7}	2.10×10^{-6}
10^4	1.00×10^{10}	1.05×10^{-1}	3.52×10^{-4}	4.46×10^{-1}	1.92×10^{-4}	6.03×10^{-4}	2.70×10^{-3}	5.40×10^{-3}	1.16×10^{-2}
10^4	1.50×10^{10}	1.14×10^0	1.05×10^{-1}	3.38×10^0	4.44×10^{-2}	1.99×10^{-2}	1.87×10^{-1}	2.87×10^{-1}	5.94×10^{-1}
10^4	2.00×10^{10}	6.76×10^0	2.92×10^0	2.12×10^1	9.40×10^{-1}	1.63×10^{-1}	2.51×10^0	3.70×10^0	7.31×10^0
10^4	2.50×10^{10}	2.56×10^1	2.75×10^1	1.02×10^2	7.01×10^0	7.08×10^{-1}	1.51×10^1	2.38×10^1	4.52×10^1
10^4	3.00×10^{10}	7.21×10^1	1.44×10^2	3.83×10^2	3.01×10^1	2.16×10^0	5.75×10^1	1.01×10^2	1.86×10^2
10^7	1.00×10^7	1.19×10^{-2}	1.00×10^{-100}	2.49×10^{-2}	1.00×10^{-100}				
10^7	4.00×10^8	1.19×10^{-2}	6.62×10^{-90}	2.50×10^{-2}	1.06×10^{-93}	1.13×10^{-79}	3.20×10^{-55}	1.04×10^{-70}	3.37×10^{-46}
10^7	7.00×10^8	1.19×10^{-2}	2.20×10^{-53}	2.52×10^{-2}	1.13×10^{-55}	6.34×10^{-52}	6.68×10^{-35}	6.07×10^{-43}	2.26×10^{-28}
10^7	1.00×10^9	1.20×10^{-2}	1.49×10^{-38}	2.58×10^{-2}	2.81×10^{-40}	9.89×10^{-38}	1.90×10^{-25}	1.02×10^{-31}	5.13×10^{-21}
10^7	2.00×10^9	1.29×10^{-2}	8.41×10^{-21}	3.29×10^{-2}	5.62×10^{-22}	6.30×10^{-20}	4.76×10^{-14}	6.30×10^{-18}	5.60×10^{-12}
10^7	3.00×10^9	1.42×10^{-2}	1.27×10^{-14}	4.32×10^{-2}	1.48×10^{-15}	1.17×10^{-13}	4.83×10^{-10}	1.91×10^{-12}	1.12×10^{-8}
10^7	5.00×10^9	1.66×10^{-2}	2.62×10^{-9}	6.31×10^{-2}	9.53×10^{-10}	2.56×10^{-8}	1.28×10^{-6}	1.89×10^{-7}	1.05×10^{-5}
10^7	1.00×10^{10}	8.91×10^{-2}	4.42×10^{-4}	3.76×10^{-1}	2.42×10^{-4}	4.82×10^{-4}	3.40×10^{-3}	4.32×10^{-3}	1.46×10^{-2}
10^7	1.50×10^{10}	1.07×10^0	1.12×10^{-1}	3.18×10^0	4.73×10^{-2}	1.87×10^{-2}	2.00×10^{-1}	2.69×10^{-1}	6.35×10^{-1}
10^7	2.00×10^{10}	6.59×10^0	3.00×10^0	2.07×10^1	9.66×10^{-1}	1.59×10^{-1}	2.58×10^0	3.60×10^0	7.52×10^0
10^7	2.50×10^{10}	2.52×10^1	2.79×10^1	1.00×10^2	7.11×10^0	6.98×10^{-1}	1.53×10^1	2.34×10^1	4.58×10^1
10^7	3.00×10^{10}	7.14×10^1	1.46×10^2	3.79×10^2	3.03×10^1	2.14×10^0	5.81×10^1	1.01×10^2	1.88×10^2
10^{11}	1.00×10^7	1.00×10^{-100}	1.14×10^4	1.00×10^{-100}	1.73×10^3	1.00×10^{-100}	8.43×10^4	1.00×10^{-100}	2.71×10^5
10^{11}	4.00×10^8	1.00×10^{-100}	1.14×10^4	1.00×10^{-100}	1.71×10^3	1.00×10^{-100}	8.45×10^4	1.00×10^{-100}	2.72×10^5
10^{11}	7.00×10^8	1.00×10^{-100}	1.14×10^4	1.00×10^{-100}	1.71×10^3	1.00×10^{-100}	8.45×10^4	1.00×10^{-100}	2.72×10^5
10^{11}	1.00×10^9	1.00×10^{-100}	1.15×10^4	1.00×10^{-100}	1.72×10^3	1.00×10^{-100}	8.45×10^4	1.00×10^{-100}	2.72×10^5
10^{11}	2.00×10^9	1.13×10^{-54}	1.26×10^4	7.40×10^{-54}	1.90×10^3	4.98×10^{-77}	8.45×10^4	1.04×10^{-74}	2.72×10^5
10^{11}	3.00×10^9	2.00×10^{-37}	1.43×10^4	1.08×10^{-36}	2.15×10^3	5.26×10^{-52}	8.39×10^4	1.21×10^{-50}	2.71×10^5
10^{11}	5.00×10^9	2.04×10^{-23}	1.70×10^4	1.12×10^{-22}	2.51×10^3	1.13×10^{-31}	8.05×10^4	8.57×10^{-31}	2.65×10^5
10^{11}	1.00×10^{10}	2.07×10^{-12}	2.35×10^4	9.38×10^{-12}	3.15×10^3	6.00×10^{-16}	7.41×10^4	5.36×10^{-15}	2.60×10^5
10^{11}	1.50×10^{10}	3.97×10^{-8}	4.83×10^4	9.66×10^{-8}	5.87×10^3	2.20×10^{-10}	7.52×10^4	3.16×10^{-9}	2.79×10^5
10^{11}	2.00×10^{10}	1.22×10^{-5}	1.05×10^5	3.12×10^{-5}	1.24×10^4	1.96×10^{-7}	7.96×10^4	4.41×10^{-6}	3.13×10^5
10^{11}	2.50×10^{10}	6.12×10^{-4}	1.87×10^5	2.18×10^{-3}	2.16×10^4	1.46×10^{-5}	8.63×10^4	4.83×10^{-4}	3.59×10^5
10^{11}	3.00×10^{10}	1.07×10^{-2}	2.87×10^5	5.35×10^{-2}	3.18×10^4	3.01×10^{-4}	9.40×10^4	1.39×10^{-2}	4.17×10^5

Table 9 Comparison of pn-QRPA calculated γ -ray heating rates and neutrino cooling rates (this work) with previous calculations due to electron capture on ^{23}Na , as function of stellar density and temperature. ADNDT99 implies (Nabi & Klapdor-Kleingrothaus 1999), OHMTS signifies (Oda et al. 1994) calculation whereas STN15 represent (Suzuki et al. 2016) results.

ρY_e (g.cm $^{-3}$)	T(K)	γ -ray heating rates (MeV.s $^{-1}$)				Neutrino cooling rates (MeV.s $^{-1}$)			
		This Work	ADNDT99	OHMTS	STN15	This Work	ADNDT99	OHMTS	STN15
10^7	1.00×10^7	$< 10^{-100}$	$< 10^{-100}$	$< 10^{-100}$	$< 10^{-100}$	$< 10^{-100}$	$< 10^{-100}$	$< 10^{-100}$	$< 10^{-100}$
	1.00×10^8	$< 10^{-100}$	$< 10^{-100}$	$< 10^{-100}$	$< 10^{-100}$	$< 10^{-100}$	$< 10^{-100}$	$< 10^{-100}$	$< 10^{-100}$
	1.00×10^9	4.17×10^{-25}	9.77×10^{-29}	5.12×10^{-29}	2.88×10^{-29}	8.93×10^{-24}	2.70×10^{-24}	8.41×10^{-25}	6.07×10^{-25}
	1.00×10^{10}	1.12×10^{-3}	7.78×10^{-4}	6.93×10^{-4}	—	5.29×10^{-3}	3.36×10^{-3}	1.89×10^{-3}	—
	3.00×10^{10}	2.32×10^1	6.28×10^0	8.99×10^1	—	1.49×10^2	8.28×10^1	1.65×10^2	—
10^8	1.00×10^7	$< 10^{-100}$	$< 10^{-100}$	$< 10^{-100}$	$< 10^{-100}$	$< 10^{-100}$	$< 10^{-100}$	$< 10^{-100}$	$< 10^{-100}$
	1.00×10^8	$< 10^{-100}$	$< 10^{-100}$	$< 10^{-100}$	$< 10^{-100}$	$< 10^{-100}$	$< 10^{-100}$	$< 10^{-100}$	$< 10^{-100}$
	1.00×10^9	7.09×10^{-19}	1.66×10^{-22}	8.69×10^{-23}	3.08×10^{-23}	1.39×10^{-17}	4.59×10^{-18}	1.41×10^{-18}	6.49×10^{-19}
	1.00×10^{10}	4.94×10^{-3}	3.48×10^{-3}	2.95×10^{-3}	—	2.36×10^{-2}	1.06×10^{-2}	7.88×10^{-3}	—
	3.00×10^{10}	2.49×10^1	6074×10^0	9.66×10^1	—	1.60×10^2	8.89×10^1	1.77×10^2	—
10^9	1.00×10^7	2.30×10^{-15}	4.14×10^{-48}	$< 10^{-100}$	$< 10^{-100}$	5.09×10^{-6}	6.57×10^{-6}	9.77×10^{-6}	2.97×10^{-7}
	1.00×10^8	2.33×10^{-15}	2.29×10^{-17}	6.59×10^{-45}	9.10×10^{-54}	5.21×10^{-6}	6.71×10^{-6}	9.93×10^{-6}	3.08×10^{-7}
	1.00×10^9	3.98×10^{-8}	9.79×10^{-9}	4.38×10^{-9}	5.20×10^{-10}	4.24×10^{-5}	1.33×10^{-4}	3.26×10^{-5}	8.09×10^{-6}
	1.00×10^{10}	1.63×10^{-1}	1.28×10^{-1}	9.16×10^{-2}	—	2.45×10^{-1}	4.16×10^{-1}	2.13×10^{-1}	—
	3.00×10^{10}	4.84×10^1	1.32×10^1	1.86×10^2	—	3.15×10^2	1.75×10^2	3.44×10^2	—
10^{10}	1.00×10^7	3.68×10^0	6.56×10^{-2}	9.29×10^0	5.86×10^0	1.53×10^1	4.95×10^0	2.36×10^1	1.46×10^1
	1.00×10^8	3.64×10^0	8.02×10^{-2}	9.29×10^0	5.82×10^0	1.51×10^1	4.95×10^0	2.36×10^1	1.45×10^1
	1.00×10^9	4.06×10^0	1.25×10^1	9.38×10^0	6.00×10^0	1.72×10^1	6.14×10^1	2.38×10^1	1.48×10^1
	1.00×10^{10}	1.16×10^1	2.45×10^1	2.74×10^1	—	2.10×10^2	1.33×10^2	5.44×10^1	—
	3.00×10^{10}	6.01×10^2	1.74×10^2	2.19×10^3	—	4.40×10^3	2.56×10^3	4.34×10^3	—
10^{11}	1.00×10^7	1.10×10^3	4.44×10^1	8.93×10^3	7.26×10^3	1.61×10^4	1.59×10^4	2.94×10^4	2.39×10^4
	1.00×10^8	1.10×10^3	5.26×10^1	8.93×10^3	7.26×10^3	1.63×10^4	1.58×10^4	2.94×10^4	2.39×10^4
	1.00×10^9	1.18×10^3	2.26×10^3	8.95×10^3	7.31×10^3	1.72×10^4	4.69×10^4	2.94×10^4	2.40×10^4
	1.00×10^{10}	4.43×10^3	2.92×10^3	1.10×10^4	—	6.99×10^4	5.37×10^4	3.21×10^4	—
	3.00×10^{10}	2.05×10^4	6.52×10^3	7.29×10^4	—	2.61×10^5	1.74×10^5	1.88×10^5	—

Table 10 Same as Table. 9 but for ^{23}Ne .

ρY_e (g.cm $^{-3}$)	T(K)	γ -ray heating rates (MeV.s $^{-1}$)				Neutrino cooling rates (MeV.s $^{-1}$)			
		This Work	ADNDT99	OHMTS	STN16	This Work	ADNDT99	OHMTS	STN16
10^7	1.00×10^7	$< 10^{-100}$	$< 10^{-100}$	$< 10^{-100}$	$< 10^{-100}$	$< 10^{-100}$	$< 10^{-100}$	$< 10^{-100}$	$< 10^{-100}$
	1.00×10^8	$< 10^{-100}$	$< 10^{-100}$	$< 10^{-100}$	$< 10^{-100}$	$< 10^{-100}$	$< 10^{-100}$	$< 10^{-100}$	$< 10^{-100}$
	1.00×10^9	4.79×10^{-45}	2.33×10^{-45}	3.40×10^{-53}	3.71×10^{-55}	1.26×10^{-43}	4.73×10^{-44}	1.10×10^{-44}	1.18×10^{-45}
	1.00×10^{10}	5.19×10^{-05}	6.24×10^{-06}	7.60×10^{-06}	—	2.93×10^{-04}	8.22×10^{-05}	3.55×10^{-05}	—
	3.00×10^{10}	1.18×10^1	3.26×10^0	1.30×10^1	—	8.49×10^{01}	1.71×10^{01}	2.36×10^{01}	—
10^8	1.00×10^7	$< 10^{-100}$	$< 10^{-100}$	$< 10^{-100}$	$< 10^{-100}$	$< 10^{-100}$	$< 10^{-100}$	$< 10^{-100}$	$< 10^{-100}$
	1.00×10^8	$< 10^{-100}$	$< 10^{-100}$	$< 10^{-100}$	$< 10^{-100}$	$< 10^{-100}$	$< 10^{-100}$	$< 10^{-100}$	$< 10^{-100}$
	1.00×10^9	1.58×10^{-38}	3.97×10^{-39}	4.88×10^{-47}	4.08×10^{-49}	2.15×10^{-37}	8.05×10^{-38}	1.73×10^{-38}	1.30×10^{-39}
	1.00×10^{10}	2.33×10^{-04}	2.81×10^{-05}	3.32×10^{-05}	—	1.32×10^{-03}	3.71×10^{-04}	3.84×10^{-04}	—
	3.00×10^{10}	1.27×10^1	3.51×10^0	1.39×10^1	—	9.14×10^{01}	1.84×10^{01}	2.54×10^{01}	—
10^9	1.00×10^7	$< 10^{-100}$	$< 10^{-100}$	$< 10^{-100}$	$< 10^{-100}$	$< 10^{-100}$	$< 10^{-100}$	$< 10^{-100}$	$< 10^{-100}$
	1.00×10^8	$< 10^{-100}$	$< 10^{-100}$	$< 10^{-100}$	$< 10^{-100}$	$< 10^{-100}$	$< 10^{-100}$	$< 10^{-100}$	$< 10^{-100}$
	1.00×10^9	5.70×10^{-26}	2.92×10^{-26}	1.81×10^{-33}	9.93×10^{-36}	7.67×10^{-24}	1.87×10^{-24}	7.53×10^{-25}	3.17×10^{-26}
	1.00×10^{10}	8.32×10^{-03}	1.15×10^{-03}	1.10×10^{-03}	—	5.14×10^{-02}	1.47×10^{-02}	4.62×10^{-03}	—
	3.00×10^{10}	2.50×10^1	6.93×10^0	2.71×10^1	—	1.80×10^2	3.62×10^1	4.95×10^1	—
10^{10}	1.00×10^7	6.84×10^{-02}	8.20×10^{-02}	$< 10^{-100}$	$< 10^{-100}$	7.40×10^{-01}	2.63×10^{-01}	1.41×10^{-02}	2.65×10^{-02}
	1.00×10^8	6.79×10^{-02}	8.15×10^{-02}	1.11×10^{-49}	2.18×10^{-55}	7.41×10^{-01}	2.61×10^{-01}	2.65×10^{-02}	1.41×10^{-02}
	1.00×10^9	6.98×10^{-02}	8.37×10^{-02}	2.61×10^{-08}	3.44×10^{-09}	7.71×10^{-01}	2.74×10^{-01}	2.75×10^{-02}	1.53×10^{-02}
	1.00×10^{10}	1.95×10^0	1.03×10^{00}	4.39×10^{-01}	—	1.68×10^0	5.65×10^0	1.16×10^{00}	—
	3.00×10^{10}	3.47×10^2	1.09×10^2	3.44×10^2	—	2.63×10^3	5.52×10^2	6.58×10^2	—
10^{11}	1.00×10^7	7.08×10^{03}	8.38×10^{03}	1.11×10^{03}	8.18×10^{02}	2.49×10^{04}	1.99×10^{04}	1.74×10^{03}	1.11×10^{03}
	1.00×10^8	7.08×10^{03}	8.39×10^{03}	1.11×10^{03}	8.22×10^{02}	2.50×10^{04}	1.99×10^{04}	1.74×10^{03}	1.11×10^{03}
	1.00×10^9	7.06×10^{03}	8.41×10^{03}	1.11×10^{03}	8.29×10^{02}	2.48×10^{04}	1.99×10^{04}	1.74×10^{03}	1.12×10^{03}
	1.00×10^{10}	6.07×10^{03}	7.33×10^{03}	2.70×10^{03}	—	2.39×10^{04}	1.72×10^{04}	1.68×10^{03}	—
	3.00×10^{10}	1.82×10^{04}	1.03×10^{04}	1.57×10^{04}	—	1.76×10^{05}	5.19×10^{04}	3.55×10^{04}	—

Table 11 Same as Table. 9 but for ^{25}Mg .

ρY_e (g.cm $^{-3}$)	T(K)	γ -ray heating rates (MeV.s $^{-1}$)				Neutrino cooling rates (MeV.s $^{-1}$)			
		This Work	ADNDT99	OHMTS	STN16	This Work	ADNDT99	OHMTS	STN16
10^7	1.00×10^7	$< 10^{-100}$	$< 10^{-100}$	$< 10^{-100}$	$< 10^{-100}$	$< 10^{-100}$	$< 10^{-100}$	$< 10^{-100}$	$< 10^{-100}$
	1.00×10^8	$< 10^{-100}$	$< 10^{-100}$	$< 10^{-100}$	$< 10^{-100}$	$< 10^{-100}$	$< 10^{-100}$	$< 10^{-100}$	$< 10^{-100}$
	1.00×10^9	1.90×10^{-25}	1.44×10^{-25}	3.06×10^{-23}	2.08×10^{-23}	5.13×10^{-21}	4.52×10^{-22}	5.30×10^{-22}	3.50×10^{-22}
	1.00×10^{10}	3.40×10^{-3}	1.94×10^{-3}	9.89×10^{-4}	—	1.46×10^{-2}	3.92×10^{-3}	3.10×10^{-3}	—
	3.00×10^{10}	5.81×10^1	3.54×10^1	9.29×10^1	—	1.88×10^2	1.08×10^2	1.69×10^2	—
10^8	1.00×10^7	$< 10^{-100}$	$< 10^{-100}$	$< 10^{-100}$	$< 10^{-100}$	$< 10^{-100}$	$< 10^{-100}$	$< 10^{-100}$	$< 10^{-100}$
	1.00×10^8	$< 10^{-100}$	$< 10^{-100}$	$< 10^{-100}$	$< 10^{-100}$	$< 10^{-100}$	$< 10^{-100}$	$< 10^{-100}$	$< 10^{-100}$
	1.00×10^9	3.23×10^{-19}	2.44×10^{-19}	4.83×10^{-17}	2.15×10^{-17}	8.39×10^{-15}	7.26×10^{-16}	8.43×10^{-16}	3.62×10^{-16}
	1.00×10^{10}	1.52×10^{-2}	8.69×10^{-3}	4.20×10^{-3}	—	6.50×10^{-2}	1.76×10^{-2}	1.29×10^{-2}	—
	3.00×10^{10}	6.24×10^1	3.80×10^1	9.98×10^1	—	2.02×10^2	1.16×10^2	1.81×10^2	—
10^9	1.00×10^7	1.53×10^{-12}	6.97×10^{-14}	3.66×10^{-5}	1.81×10^{-5}	9.71×10^{-3}	4.45×10^{-4}	6.70×10^{-4}	2.31×10^{-4}
	1.00×10^8	1.54×10^{-12}	7.00×10^{-14}	3.66×10^{-5}	1.97×10^{-5}	9.79×10^{-3}	4.47×10^{-4}	6.71×10^{-4}	2.55×10^{-4}
	1.00×10^9	6.30×10^{-6}	2.38×10^{-6}	4.20×10^{-5}	2.59×10^{-5}	1.21×10^{-2}	5.50×10^{-4}	8.41×10^{-4}	3.88×10^{-4}
	1.00×10^{10}	5.87×10^{-1}	3.33×10^{-1}	1.32×10^{-1}	—	2.36×10^0	6.92×10^{-1}	3.52×10^{-1}	—
	3.00×10^{10}	1.23×10^2	7.46×10^1	1.92×10^2	—	3.98×10^2	2.29×10^2	3.51×10^2	—
10^{10}	1.00×10^7	7.43×10^1	1.20×10^1	1.54×10^1	8.85×10^{00}	2.65×10^2	3.61×10^1	2.47×10^1	1.68×10^1
	1.00×10^8	7.41×10^1	1.20×10^1	1.54×10^1	8.85×10^{00}	2.63×10^2	3.58×10^1	2.47×10^1	1.68×10^1
	1.00×10^9	7.53×10^1	1.22×10^1	1.55×10^1	9.12×10^{00}	2.65×10^2	3.63×10^1	2.49×10^1	1.72×10^1
	1.00×10^{10}	1.96×10^2	6.87×10^1	4.37×10^1	—	5.71×10^2	1.82×10^2	7.36×10^1	—
	3.00×10^{10}	1.77×10^3	1.05×10^3	2.26×10^3	—	5.87×10^3	3.45×10^3	4.44×10^3	—
10^{11}	1.00×10^7	8.43×10^4	3.08×10^4	1.46×10^4	1.03×10^4	2.71×10^5	7.94×10^4	3.93×10^4	3.07×10^4
	1.00×10^8	8.49×10^4	3.13×10^4	1.46×10^4	1.03×10^4	2.73×10^5	8.05×10^4	3.93×10^4	3.07×10^4
	1.00×10^9	8.45×10^4	3.10×10^4	1.47×10^4	1.03×10^4	2.72×10^5	8.00×10^4	3.93×10^4	3.08×10^4
	1.00×10^{10}	7.41×10^4	2.96×10^4	1.67×10^4	—	2.60×10^5	9.84×10^4	4.25×10^4	—
	3.00×10^{10}	9.40×10^4	5.28×10^4	7.60×10^4	—	4.17×10^5	2.73×10^5	1.92×10^5	—

Table 12 Same as Table. 9 but for ^{25}Na .

ρY_e (g.cm $^{-3}$)	T(K)	γ -ray heating rates (MeV.s $^{-1}$)				Neutrino cooling rates (MeV.s $^{-1}$)			
		This Work	ADNDT99	OHMTS	STN16	This Work	ADNDT99	OHMTS	STN16
10^7	1.00×10^7	$< 10^{-100}$	$< 10^{-100}$	$< 10^{-100}$	$< 10^{-100}$	$< 10^{-100}$	$< 10^{-100}$	$< 10^{-100}$	$< 10^{-100}$
	1.00×10^8	$< 10^{-100}$	$< 10^{-100}$	$< 10^{-100}$	$< 10^{-100}$	$< 10^{-100}$	$< 10^{-100}$	$< 10^{-100}$	$< 10^{-100}$
	1.00×10^9	2.81×10^{-40}	5.07×10^{-39}	3.98×10^{-46}	5.01×10^{-47}	1.49×10^{-38}	3.49×10^{-38}	3.98×10^{-39}	2.51×10^{-39}
	1.00×10^{10}	2.42×10^{-4}	9.18×10^{-5}	3.48×10^{-5}	—	4.42×10^{-4}	3.62×10^{-4}	7.23×10^{-5}	—
	3.00×10^{10}	3.03×10^1	1.10×10^1	1.79×10^1	—	1.46×10^2	1.07×10^2	3.53×10^1	—
10^8	1.00×10^7	$< 10^{-100}$	$< 10^{-100}$	$< 10^{-100}$	$< 10^{-100}$	$< 10^{-100}$	$< 10^{-100}$	$< 10^{-100}$	$< 10^{-100}$
	1.00×10^8	$< 10^{-100}$	$< 10^{-100}$	$< 10^{-100}$	$< 10^{-100}$	$< 10^{-100}$	$< 10^{-100}$	$< 10^{-100}$	$< 10^{-100}$
	1.00×10^9	4.75×10^{-34}	8.59×10^{-33}	6.58×10^{-40}	6.31×10^{-41}	2.50×10^{-32}	5.90×10^{-32}	5.87×10^{-33}	2.99×10^{-33}
	1.00×10^{10}	1.08×10^{-3}	4.12×10^{-4}	1.53×10^{-4}	—	1.99×10^{-3}	1.62×10^{-3}	3.16×10^{-4}	—
	3.00×10^{10}	3.25×10^1	1.18×10^1	1.91×10^1	—	1.56×10^2	1.15×10^2	3.08×10^1	—
10^9	1.00×10^7	$< 10^{-100}$	$< 10^{-100}$	$< 10^{-100}$	$< 10^{-100}$	$< 10^{-100}$	$< 10^{-100}$	$< 10^{-100}$	$< 10^{-100}$
	1.00×10^8	$< 10^{-100}$	$< 10^{-100}$	$< 10^{-100}$	$< 10^{-100}$	$< 10^{-100}$	$< 10^{-100}$	$< 10^{-100}$	$< 10^{-100}$
	1.00×10^9	3.00×10^{-20}	4.31×10^{-19}	3.86×10^{-26}	1.26×10^{-27}	1.59×10^{-18}	3.17×10^{-18}	2.96×10^{-19}	6.75×10^{-20}
	1.00×10^{10}	3.94×10^{-2}	1.54×10^{-2}	5.51×10^{-3}	—	7.80×10^{-2}	6.46×10^{-2}	1.09×10^{-2}	—
	3.00×10^{10}	6.37×10^1	2.32×10^1	3.72×10^1	—	3.08×10^2	2.26×10^2	6.01×10^1	—
10^{10}	1.00×10^7	3.45×10^{-1}	1.17×10^1	3.05×10^{-1}	7.59×10^{-2}	6.38×10^{-1}	2.65×10^0	2.14×10^{-1}	3.03×10^{-2}
	1.00×10^8	3.46×10^{-1}	1.17×10^1	3.05×10^{-1}	7.41×10^{-2}	6.41×10^{-1}	2.65×10^0	2.14×10^{-1}	2.97×10^{-2}
	1.00×10^9	3.63×10^{-1}	1.87×10^{-1}	3.00×10^{-1}	7.76×10^{-2}	6.85×10^{-1}	3.02×10^1	4.71×10^{-1}	2.60×10^{-1}
	1.00×10^{10}	7.05×10^{00}	4.53×10^0	3.16×10^{00}	—	2.48×10^1	3.31×10^1	5.87×10^{00}	—
	3.00×10^{10}	8.43×10^2	3.08×10^2	4.76×10^2	—	4.50×10^3	3.33×10^3	8.07×10^2	—
10^{11}	1.00×10^7	1.73×10^3	2.04×10^3	4.16×10^3	3.80×10^3	1.14×10^4	2.58×10^4	1.14×10^4	9.04×10^3
	1.00×10^8	1.71×10^3	2.02×10^3	4.16×10^3	3.80×10^3	1.14×10^4	2.55×10^4	1.14×10^4	9.03×10^3
	1.00×10^9	1.72×10^3	1.51×10^3	4.13×10^3	3.89×10^3	1.15×10^4	2.10×10^4	1.15×10^4	9.45×10^3
	1.00×10^{10}	3.15×10^3	1.37×10^3	4.98×10^3	—	2.35×10^4	3.29×10^4	1.28×10^4	—
	3.00×10^{10}	3.18×10^4	4.57×10^4	2.25×10^4	—	2.87×10^5	2.29×10^5	4.65×10^4	—

Table 13 Comparison of pn-QRPA calculated γ -ray heating rates and neutrino cooling rates (this work) with previous calculations, due to β^- -decay from ^{20}O , as function of stellar density and temperature. OHMTS signifies (Oda et al. 1994) calculation whereas STN15 represent (Suzuki et al. 2016) results.

ρY_e (g.cm $^{-3}$)	T(K)	γ -ray heating rates (MeV.s $^{-1}$)			Neutrino cooling rates (MeV.s $^{-1}$)		
		This Work	OHMTS	STN16	This Work	OHMTS	STN16
10^1	1.00×10^7	6.12×10^{-2}	5.26×10^{-2}	—	$< 10^{-100}$	7.74×10^{-2}	—
	1.00×10^8	6.12×10^{-2}	5.26×10^{-2}	—	$< 10^{-100}$	7.74×10^{-2}	—
	1.00×10^9	6.12×10^{-2}	5.26×10^{-2}	—	1.58×10^{-26}	7.74×10^{-2}	—
	1.00×10^{10}	1.46×10^0	1.10×10^0	—	6.37×10^{-3}	1.58×10^0	—
	3.00×10^{10}	2.16×10^2	7.92×10^2	—	1.06×10^2	1.04×10^3	—
10^4	1.00×10^7	6.12×10^{-2}	5.26×10^{-2}	—	$< 10^{-100}$	7.74×10^{-2}	—
	1.00×10^8	6.12×10^{-2}	5.26×10^{-2}	—	$< 10^{-100}$	7.74×10^{-2}	—
	1.00×10^9	6.12×10^{-2}	5.26×10^{-2}	—	1.41×10^{-27}	7.74×10^{-2}	—
	1.00×10^{10}	1.46×10^0	1.10×10^0	—	6.37×10^{-3}	1.58×10^0	—
	3.00×10^{10}	2.16×10^2	7.92×10^2	—	1.06×10^2	1.04×10^3	—
10^7	1.00×10^7	3.69×10^{-2}	4.06×10^{-2}	4.36×10^{-2}	$< 10^{-100}$	5.15×10^{-2}	5.62×10^{-2}
	1.00×10^8	3.69×10^{-2}	4.06×10^{-2}	4.42×10^{-2}	$< 10^{-100}$	5.15×10^{-2}	5.67×10^{-2}
	1.00×10^9	3.79×10^{-2}	4.10×10^{-2}	4.36×10^{-2}	1.43×10^{-32}	5.25×10^{-2}	5.70×10^{-2}
	1.00×10^{10}	1.18×10^0	9.02×10^{-1}	—	5.09×10^{-3}	1.32×10^0	—
	3.00×10^{10}	2.14×10^2	7.87×10^2	—	1.05×10^2	1.03×10^3	—
10^{11}	1.00×10^7	$< 10^{-100}$	$< 10^{-100}$	$< 10^{-100}$	$< 10^{-100}$	$< 10^{-100}$	$< 10^{-100}$
	1.00×10^8	$< 10^{-100}$	$< 10^{-100}$	$< 10^{-100}$	$< 10^{-100}$	$< 10^{-100}$	$< 10^{-100}$
	1.00×10^9	$< 10^{-100}$	$< 10^{-100}$	$< 10^{-100}$	$< 10^{-100}$	$< 10^{-100}$	$< 10^{-100}$
	1.00×10^{10}	3.06×10^{-11}	2.05×10^{-10}	—	6.41×10^{-15}	5.34×10^{-10}	—
	3.00×10^{10}	3.31×10^{-2}	1.26×10^{-1}	—	1.46×10^{-2}	1.66×10^{-1}	—